NASA Technical Memorandum 4222

Real-Time Aerodynamic Heating and Surface Temperature Calculations for Hypersonic Flight Simulation

Robert D. Quinn and Leslie Gong

AUGUST 1990

NASA Technical Memorandum 4222

Real-Time Aerodynamic Heating and Surface Temperature Calculations for Hypersonic Flight Simulation

Robert D. Quinn and Leslie Gong
Ames Research Center
Dryden Flight Research Facility
Edwards, California

National Aeronautics and
Space Administration
Office of Management
Scientific and Technical
Information Division

1990

ABSTRACT

A real-time heating algorithm has been derived and installed on the Ames Research Center Dryden Flight Research Facility real-time flight simulator. This program can calculate two- and three-dimensional stagnation point surface heating rates and surface temperatures. The two-dimensional calculations can be made with or without leading-edge sweep. In addition, upper and lower surface heating rates and surface temperatures for flat plates, wedges, and cones can be calculated. Laminar or turbulent heating can be calculated, with boundary-layer transition made a function of free-stream Reynolds number and free-stream Mach number. Real-time heating rates and surface temperatures calculated for a generic hypersonic vehicle are presented and compared with more exact values computed by a batch aeroheating program. As these comparisons show, the heating algorithm used on the flight simulator calculates surface heating rates and temperatures well within the accuracy required to evaluate flight profiles for acceptable heating trajectories.

INTRODUCTION

The procedure usually used to evaluate the heating severity of flight profiles is obtaining the flight profiles from a real-time flight simulator and coding the profile to be entered into an aerodynamic heating program to calculate surface heating rates and surface temperatures. If the heating rates or temperatures were too high, then another profile was generated by the flight simulator and used to compute new heating rates and temperatures. This procedure was continued until acceptable heating trajectories were established. The time required to evaluate the flight trajectories would be significantly reduced if the heating rates and temperatures could be calculated in real time on the flight simulator.

This paper presents equations and tables for a real-time heating method that has been incorporated on the Ames Research Center Dryden Flight Research Facility (Ames-Dryden) flight simulator. The real-time surface heating rates and surface temperatures calculated by this program are presented for selected locations on a generic hypersonic vehicle, and these results are compared with values computed by an aeroheating computer program. The Ames-Dryden flight simulator is described in the appendix, prepared by Lawrence J. Schilling.

NOMENCLATURE

Symbols

A_1	turbulent correction factor
A_2	laminar correction factor
C_m	transition Mach number coefficient
$C_{p,w}$	specific heat of the surface material, Btu/lbm °R
C_1	constant in equation 15
C_3	constant in equation 18
C_5	transformation value for conical flow
F	radiation geometry factor, 1.0
H	enthalpy, Btu/lbm
H^*	reference enthalpy, Btu/lbm
h	local heat transfer coefficient, lbm/ft^2 sec

h_0	flat-plate heat transfer coefficient at zero angle of attack, lbm/ft^2 sec
h_α	heat transfer coefficient due to angle of attack and wedge or cone angle, lbm/ft^2 sec
K_1	three-dimensional stagnation factor
K_2	two-dimensional stagnation factor
M	Mach number
P	static pressure, lb/ft^2
Pr	Prandtl number, assumed to be 0.70 for calculations
q	heating rate, Btu/ft^2 sec
R	body nose radius, ft
Re	Reynolds number, $\rho U x/\mu$
Re_T	transition Reynolds number, $\rho U x/\mu$
T	temperature, °R or °F
T^*	reference temperature, °R
$\dot{T}_w$	rate of change of surface temperature, °R/sec
t	time, sec
U	velocity, ft/sec
x	surface distance from leading edge of wing or nose of fuselage, ft
$\left(\frac{dU}{dx}\right)_{x=0}$	stagnation velocity gradient

Greek

α	angle of attack, deg
β	radiation factor, $\sigma\varepsilon$ F, Btu/ft^2 sec °R^4
δ	wedge half angle, deg
ε	emissivity
θ	cone half angle, deg
Λ	wing leading-edge sweep angle, deg
μ	dynamic viscosity, lb/ft sec
ρ	density of air, lbm/ft^3
ρ_w	density of surface material, lbm/ft^3
σ	Stefan-Boltzman constant, 4.78 Btu/ft^2 sec °R^4
τ	wall or skin thickness, ft
ϕ	circumferential angle, zero on cone centerline, deg

Subscripts

R	boundary-layer recovery
st	stagnation
T	transition

w wall

∞ free stream

AERODYNAMIC HEATING ALGORITHM

A real-time heating algorithm has been developed and installed on the Ames-Dryden flight simulator. It was used to obtain surface heating rates and surface temperatures for hypersonic vehicles. This program can calculate three-dimensional stagnation heating rates and temperatures, and two-dimensional stagnation heating rates and temperatures with and without leading-edge sweep. It can also calculate lower and upper surface heating rates and temperatures for flat plates, wedges, and cones. Laminar and turbulent heating rates and temperatures can be calculated, with boundary-layer transition controlled as a function of free-stream Reynolds number and free-stream Mach number. The program uses time histories of altitude, Mach number or velocity, and angle of attack along with atmospheric tables to obtain the free-stream properties required to make the calculations. Other inputs required to make the calculations are the values in Tables 1–4, constants C_1 and C_3, heat capacity ($\rho_w C_{p,w} \tau$) and an initial value for the wall temperature (T_w). The constants C_1 and C_3 default to 1 if values are not specified.

Heating Equation for Stagnation Point Calculations

The basic equation used to compute the surface temperatures and heating rates for stagnation point calculations is (Quinn and Palitz, 1966)

$$q = (\rho_w C_{p,w} \tau)\dot{T}_w = h(H_{st} - H_w) - \beta T_w^4 \tag{1}$$

for three-dimensional stagnation points or unswept leading edges, and for swept leading edges

$$q = (\rho_w C_{p,w} \tau)\dot{T}_w = h(H_R - H_w) - \beta T_w^4 \tag{2}$$

To obtain good surface temperatures and, to a lesser extent, good surface heating rates, proper engineering judgment must be exercised to determine the heat capacity for these equations. Since the values of the specific heat of the surface material ($C_{p,w}$) and the density of the surface material (ρ_w) are thermal properties of the material, the only way to vary the heat capacity significantly is to change the value of the material thickness (τ). For metallic surfaces, the thickness of the skin will give satisfactory results. For surfaces that are insulated with low conductivity insulation (such as the space shuttle), a material thickness should be used that will result in a heat capacity of approximately 0.1 Btu/ft^2 °R. To solve equations 1 and 2, the heat transfer coefficient (h) must be determined. The heat transfer coefficient is calculated for three-dimensional flow by

$$h = 0.94\, K_1 (\rho_{st}\mu_{st})^{0.4} (\rho_w \mu_w)^{0.1} \sqrt{(dU/dx)_{x=0}} \tag{3}$$

and for two-dimensional flow by

$$h = 0.706\, K_2 (\rho_{st}\mu_{st})^{0.4} (\rho_w \mu_w)^{0.1} \sqrt{(dU/dx)_{x=0}} \tag{4}$$

Equations 3 and 4 are modified versions of the equations given by Fay and Riddell (1958). Usually, to solve equations 1–4 local flow conditions behind a normal shock wave must be calculated. However, to minimize computation time, a method has been developed which allows satisfactory solutions to these equations using only the free-stream flow conditions along with a table of values for K_1 and K_2. Equations 1–4 are solved by the program using the following computational steps

$$H_{st} = H_\infty + \frac{U_\infty^2 \cos^2 \Lambda}{50{,}103} \tag{5}$$

for three-dimensional calculations, and

$$H_R = H_\infty + \frac{U_\infty^2 \cos^2 \Lambda}{50{,}103} + 0.85 \frac{U_\infty^2 \sin^2 \Lambda}{50{,}103} \tag{6}$$

for two-dimensional calculations.

$$\left(\frac{dU}{dx}\right)_{x=0} = \frac{1}{R}\sqrt{\frac{(7M_\infty^2 \cos^2 \Lambda - 1)(M_\infty^2 \cos^2 \Lambda + 5)}{M_\infty^2 \cos^2 \Lambda}\left(\frac{P_\infty}{\rho_\infty}\right)} \tag{7}$$

$$\rho_{st}\mu_{st} = \rho_\infty \mu_\infty \left(\frac{6M_\infty^2 \cos^2 \Lambda}{M_\infty^2 \cos^2 \Lambda + 5}\right)\left(\frac{T_{st}}{T_\infty}\right)^{0.75} \tag{8}$$

$$\mu_\infty = 1.05 \times 10^{-7}(T_\infty)^{0.75} \tag{9}$$

$$\mu_w = 1.05 \times 10^{-7}(T_w)^{0.75} \tag{10}$$

$$P_w \approx P_{st} \approx P_\infty \frac{[(7M_\infty^2 \cos^2 \Lambda) - 1]}{6} \tag{11}$$

$$\rho_w = \frac{P_w}{53.3\, T_w} \tag{12}$$

For three-dimensional stagnation point calculations, the sweep angle (Λ) in the above equations will be zero. Values of H_∞, H_w, T_R, and T_{st} are obtained by linear interpolation from table 1 (Hansen, 1959). Values for K_1 and K_2 are determined by linear interpolation from table 2.

Heating Equation for Small or Zero Pressure Gradient Surfaces

The basic equation used to calculate the surface heating rates and surface temperatures for small or zero pressure gradient surfaces can be written as (Quinn and Palitz, 1966)

$$\dot{q} = (\rho_w C_{p,w} \tau)\dot{T}_w = h(H_R - H_w) - \beta T_w^4 \tag{13}$$

The value given to the heat capacity is very important. Since the values of ρ_w and $C_{p,w}$ are thermal properties of the material and cannot be changed, the proper value of the heat capacity can only be obtained by judiciously selecting the value of τ. For metallic surfaces, good results can be obtained by setting τ equal to the skin thickness. For insulated surfaces, a value of τ should be selected that will result in a heat capacity of approximately 0.1 Btu/ft^2 °R.

Calculating the heat transfer coefficient from equation 13 usually requires calculating the local flow conditions. However, to minimize computation time and thus obtain real-time solutions, a method has been developed that produces satisfactory surface heating rates and surface temperatures for flat plates, wedges, or cones using only the free-stream flow conditions.

The heat transfer coefficient is written as

$$h = C_5(h_o + h_\alpha) \tag{14}$$

where h_o is the heat transfer coefficient for a flat plate at zero angle of attack and h_α is that portion of the total heat transfer coefficient caused by the angle of attack and wedge or cone angles. The constant C_5 is the transformation

value to correct two-dimensional heat transfer coefficients to conical flow values. For turbulent flow C_5 is 1.15, and for laminar flow C_5 is 1.73.

For turbulent flow the following equations are used to calculate the heat transfer coefficient

$$h_o = \left[\frac{C_1(0.0375)(\rho_\infty U_\infty)^{0.8}(\mu)^{0.2}}{x^{0.2}}\right]\left(\frac{T_\infty}{T^*}\right)^{0.65} \tag{15}$$

$$h_\alpha = A_1\left[\frac{(\rho_\infty U_\infty)^{0.8}}{x^{0.2}}\right](\delta + \alpha) \tag{16}$$

for lower surfaces, and

$$h_\alpha = A_1\left[\frac{(\rho_\infty U_\infty)^{0.8}}{x^{0.2}}\right](\delta - \alpha) \tag{17}$$

for upper surfaces.

Equation 15 is based on the Blasius incompressible resistance formula (Schilchting, 1960) and is related to heat transfer by a modified Reynolds analogy. The modified Reynolds analogy used was $(\mathrm{Pr})^{-2/3}$ where Pr is the Prandtl number and was assumed to be a constant of 0.7. Compressibility effects were accounted for by Eckert's reference enthalpy method (Eckert, 1960, and Zoby, Moss, and Sutton, 1981). The constant C_1 is an empirical value used to adjust the heat transfer coefficient to account for the approximation used in developing equation 15. The best results were obtained when C_1 was given a value of 1.0 for upper surface calculations and 0.90 for lower surface calculations. Equations 16 and 17 represent the difference between the heat transfer coefficient calculated using free-stream flow conditions and the values that would be calculated using local flow properties.

For laminar flow the following equations were used

$$h_o = C_3(0.421)\left(\frac{\rho_\infty U_\infty \mu_\infty}{x}\right)^{0.5}\left(\frac{T_\infty}{T^*}\right)^{0.125} \tag{18}$$

with

$$h_\alpha = A_2\left(\frac{\rho_\infty U_\infty}{x}\right)^{0.5}(\delta + \alpha) \tag{19}$$

for lower surfaces, and

$$h_\alpha = A_2\left(\frac{\rho_\infty U_\infty}{x}\right)^{0.5}(\delta - \alpha) \tag{20}$$

for upper surfaces.

Equation 18 was derived by relating skin friction to heat transfer through a modified Reynolds analogy. The modified Reynolds analogy used was $(\mathrm{Pr})^{-2/3}$ and Pr was assumed to have a constant value of 0.7. The skin friction coefficient was calculated from the Blasius incompressible equation (Schilchting, 1960). Compressibility and wall temperature effects were accounted for by Eckert's reference enthalpy method (Eckert, 1960). The constant C_3 was used to modify equation 18 to account for the approximation made in deriving the equation. For the calculations in this report, a value of 1.0 was used for C_3 in the upper surface calculations and 0.95 was used in the lower surface calculations. Equations 19 and 20 are the laminar flow equivalents of equations 16 and 17. In equations 16 and 19 the value for the wedge angle plus angle of attack $(\delta + \alpha)$ is limited to 40°, and in equations 17 and 20 the value of the wedge angle minus the angle of attack $(\delta - \alpha)$ is limited to $-10°$.

Auxiliary program steps necessary to complete the calculation are

$$Re_\infty = \rho_\infty U_\infty x/\mu_\infty \tag{21}$$

$$\mu_\infty = 1.05 \times 10^{-7}(T_\infty)^{0.75} \tag{22}$$

$$H_R = H_\infty + 0.85\frac{U_\infty^2}{50{,}103} \tag{23}$$

for laminar flow, and

$$H_R = H_\infty + 0.89\frac{U_\infty^2}{50{,}103} \tag{24}$$

for turbulent flow.

$$H^* = H_\infty + 0.5(H_w - H_\infty) + 0.22(H_R - H_\infty) \tag{25}$$

$$H_w = f(T_w, P_\infty) \tag{26}$$

$$H_\infty = f(T_\infty, P_\infty) \tag{27}$$

$$T^* = f(H^*, P_\infty) \tag{28}$$

Using linear interpolation, values for H_w, H_∞, and T^* are obtained from table 1, and values of A_1 and A_2 are obtained from tables 3 and 4 respectively.

Boundary-Layer Transition

Boundary-layer transition is usually based on local flow conditions (such as local Reynolds number and local Mach number). However, because the local flow conditions were not calculated in the real-time heating program, a transition method based on free-stream Reynolds number (Re_∞) and free-stream Mach number (M_∞) has been developed. The following transition criteria were used in the real-time heating program.

If $\log Re_\infty \leq [\log Re_T + C_m(M_\infty)]$

then laminar flow was assumed.

If $\log Re_\infty > [\log Re_T + C_m(M_\infty)]$

then turbulent flow was assumed.

The user must enter the transition Mach number coefficient and the log of the transition Reynolds number into the real-time heating program. These may be changed at the beginning of each new flight profile simulation, but cannot be varied during the simulation. Values of the log Re_T and C_m depend on the type of flow, angle of attack, leading-edge sweep angle, and leading-edge or nose bluntness. Table 5 lists the values that have been estimated to produce satisfactory transition results.

RESULTS AND DISCUSSION

The results in this report were obtained from calculations based on the flight profile in figure 1, which shows time histories of velocity, altitude, and angle of attack. This profile is typical for hypersonic airbreathing vehicles. The maximum velocity is approximately 17,000 ft/sec at an altitude of approximately 150,000 ft, and this profile includes hypersonic maneuvering flight.

To establish the accuracy of the heating rates and temperatures calculated by the aerodynamic heating algorithm, the surface heating rates and surface temperatures calculated in real time were compared to values calculated by an in-house batch computer program called AEROHEATING. This program solves the one-dimensional thin-skin heating equation (equations 1, 2, and 13) and computes time histories of heat transfer coefficients, surface temperatures, heating rates, skin friction, and other pertinent parameters. This program uses the theory of van Driest (1956), Eckert's reference enthalpy method (Eckert 1960), and the theory of Fay and Riddell (1958) to compute local heat transfer coefficients. In the present analysis, the theory of van Driest was used to compute turbulent heat transfer coefficients, Eckert's reference enthalpy method was used to compute laminar heat transfer coefficients, and the theory of Fay and Riddell was used to calculate stagnation point heat transfer coefficients. Local flow properties needed to solve the heat transfer equations were calculated by the AEROHEATING program. The theory of van Driest and Eckert's reference enthalpy method predict heat transfer coefficients that are in good agreement with measured data (Zoby, Moss, and Sutton, 1981; Quinn and Gong, 1980; and Ko, Quinn, and Gong, 1986). The theory of Fay and Riddell predicts stagnation point heat transfer with good accuracy (Rose and Stark, 1958).

Surface heating rates and surface temperatures calculated in real time on the flight simulator are compared with values calculated by the AEROHEATING program in figures 2–5. The heating capacity used in all cases was 0.5 Btu/ft^2 °R. These figures show plots of heating rates and temperature as a function of flight profile time. Figures 2–5 also show when boundary-layer transition occurred.

Figure 2 shows comparisons for stagnation heating rates and temperatures. Figures 2(a) and (b) show the results for a three-dimensional stagnation point. Figures 2(c) and (d) show results for a two-dimensional stagnation point with a 0°-leading-edge sweep, and figures 2(e) and (f) show results for a two-dimensional stagnation point with a leading-edge sweep angle of 60°. The agreement between the real-time heating rates and temperatures and the values calculated from the AEROHEATING program is very good.

Figure 3 shows heating rates and temperatures calculated for a zero pressure gradient surface with a leading-edge sweep angle of 0° and a wedge angle of 0° for flow distances of 3, 6, 12, and 24 ft. Figures 3(a)–(h) show results for a lower surface, and figures 3(i)–(p) show results for an upper surface. The difference between the results from the real-time simulator and from the AEROHEATING program are small and the overall agreement is good.

Figure 4 shows the results of calculations made for a zero pressure gradient surface with a leading-edge sweep of 60° and a wedge angle of 10°. These calculations were also made for flow distances of 3, 6, 12, and 24 ft. Figures 4(a)–(h) show lower surface results, and figures 4(i)–(p) show upper surface results. Again, the agreement between the results from the real-time flight simulator and the results from the AEROHEATING program is good.

Figure 5 shows calculations made for a cone with a semi-vertex angle of 10°. These calculations were made for flow distances of 3, 6, 12, and 24 ft. Figures 5(a)–(h) show the results for the lower surface and figures 5(i)–(p) show the results for the upper surface. Between 600 and 1200 sec, the real-time results are slightly higher than the results from the AEROHEATING program. But between 1500 and 2000 sec, they are lower than the results from the AEROHEATING program. The agreement of the real-time heating rates and temperatures with the values calculated by the AEROHEATING program, however, is still considered acceptable. Although the results were calculated using the flight simulation profile shown in figure 1, the aerodynamic heating algorithm should produce good results when using other flight simulation profiles for hypersonic airbreathing vehicles.

CONCLUDING REMARKS

An aerodynamic heating algorithm has been developed and installed on the Ames Research Center Dryden Flight Research Facility real-time flight simulator. Surface heating rates and surface temperatures have been calculated in real time for a generic hypersonic flight profile at selected locations on a hypothetical hypersonic vehicle. These real-time heating rates and temperatures were compared with values predicted by the AEROHEATING program. These comparisons showed that the surface heating rates and surface temperatures predicted by the real-time aerodynamic

heating algorithm are within the accuracy required to evaluate the heating severity of flight trajectories. Therefore, this method can be used for thermal control of flight simulation trajectories for hypersonic airbreathing vehicles.

Ames Research Center
Dryden Flight Research Facility
National Aeronautics and Space Administration
Edwards, California, March 2, 1990

APPENDIX
REAL-TIME HYPERSONIC SIMULATION

By Lawrence J. Schilling

Real-time, piloted hypersonic simulation at NASA Ames-Dryden is conducted from a fixed-base cockpit using a facsimile of the shuttle instrument panel. The simulation software is hosted on a pair of Gould (Encore Computer Corp., Fort Lauderdale, FL.) computers (a 32/9780 and a 32/6750) joined with shared memory. The simulator is also supported by two eight-channel strip chart recorders, a 30 by 30-in. map board, a 10 by 14-in. x-y plotter, and an interactive user terminal. A single "out the window" visual scene is generated with a silicon graphics IRIS 4D/80GT (Silcon Graphics, Inc., Mountain View, CA). Two monitors with engineering displays are driven by a MassComp 5400 (Concurrent Computer Corp., Westford, MA) workstation. One of these monitors provides graphical and pictorial information from the aerothermal heating model, including an illustration of the vehicle which changes color as surface temperatures change. The second monitor provides vehicle groundtracking over a map of the continental United States.

This simulation is primarily a development, familiarization, investigation, and evaluation tool. It provides a high-fidelity engineering environment which is flexible and responsive to the needs of the user. The simulation is completely controlled by the pilot or engineer in the cockpit station. Selected parameters can be recorded in real time for later display and analysis.

The simulator incorporates many user–machine interfaces. For example, from his seat the pilot can change any initial condition, select auto-trim, wind, and gust models, start or stop strip charts, and control whether the simulation is in the reset, operate, or hold mode. The user can select from more than 50 interactive alphanumeric displays which are updated dynamically and contain virtually all parameters of interest. The user can modify the initial conditions, vehicle characteristics, or control system parameters, specify parameters for real-time recording and routing to the strip charts, control simulation and vehicle modes, and perform many functions through interaction with these displays. A hard copy of any display is readily available.

The simulation software is written in FORTRAN 77. It is highly modular and consists of both generic and vehicle-specific models. The simulation features full six-degree-of-freedom oblate earth kinematic and gravity models, simple wind, gust, and atmospheric models, an aerodynamic heating model, a sonic boom overpressure model, vehicle specific aerodynamic, propulsion, actuator, and mass property models, and control augmentation system and guidance algorithms. As currently configured, the airframe dynamics are computed at 100 Hz. The aerothermal model is executed once a second.

REFERENCES

Eckert, Ernst R.G., *Survey of Boundary Layer Heat Transfer at High Velocities and High Temperatures*, WADC Tech. Rep. 59-624, Wright-Patterson AFB, Ohio, 1960.

Fay, J.A., and F.R. Riddell, "Theory of Stagnation Point Heat Transfer in Dissociated Air," *J. Aeronautical Sciences*, vol. 25, no. 2, Feb. 1958, pp. 73–85, 121.

Hansen, C. Fredrick, *Approximation for the Thermo-Dynamics and Transport Properties of High-Temperature Air*, NASA TR R-50, 1959.

Ko, William L., Robert D. Quinn, and Leslie Gong, *Finite-Element Reentry Heat-Transfer Analysis of Space Shuttle Orbiter*, NASA TP-2657, 1986.

Quinn, Robert D., and Leslie Gong, *In-Flight Boundary-Layer Measurements on a Hollow Cylinder at a Mach Number of 3.0*, NASA TP-1764, 1980.

Quinn, Robert D., and Murray Palitz, *Comparison of Measured and Calculated Turbulent Heat Transfer on the X-15 Airplane at Angles of Attack up to 19.0°*, NASA TMX-1291, 1966.

Rose, P.H., and W.I. Stark, "Stagnation Point Heat-Transfer Measurements in Dissociated Air," *J. Aeronautical Sciences*, vol. 25, no. 2, Feb. 1958, pp. 86–97.

Schilchting, Hermann, *Boundary Layer Theory*, translated by J. Kestin, fourth ed., McGraw Hill Book Co., Inc., New York, 1960.

van Driest, E.R., "The Problem of Aerodynamic Heating," *Aeronautical Engineering Review*, vol. 15, no. 10, Oct. 1956, pp. 26–41.

Zoby, E.V., J.N. Moss, and K. Sutton, "Approximate Convective-Heating Equations for Hypersonic Flows," *J. Spacecraft and Rockets*, vol. 18, no. 1, Jan./Feb. 1981, pp. 64–70. Also available as AIAA 79-1078.

Table 1. Enthalpy of air, BTU/lbm.

T,	Pressure, lb/ft^2					
°R	21,160	2,116	211.6	21.16	2.116	0.212
0	0	0	0	0	0	0
450	108	108	108	108	108	108
900	217	217	217	217	217	217
1,350	334	334	334	334	334	334
1,800	451	451	451	451	451	451
2,250	578	578	578	578	578	578
2,700	704	704	704	704	704	704
3,150	836	836	836	836	836	864
3,600	968	968	971	978	1,004	1,091
4,050	1,111	1,111	1,131	1,175	1,280	1,625
4,500	1,244	1,264	1,322	1,486	1,894	2,771
4,950	1,379	1,438	1,595	1,984	2,682	2,838
5,400	1,578	1,706	2,040	2,641	2,968	3,038
5,850	1,788	2,017	2,456	3,016	3,170	3,236
6,300	2,051	2,481	2,970	3,279	3,360	3,467
6,750	2,352	2,874	3,346	3,498	3,637	3,938
7,200	2,740	3,321	3,554	3,724	3,995	4,844
7,650	3,103	3,659	3,841	4,068	4,644	6,688
8,100	3,471	3,807	4,081	4,514	5,849	9,305
8,550	3,782	4,132	4,441	5,262	7,890	12,036
9,000	4,013	4,400	4,916	6,457	10,261	14,452
9,450	4,392	4,710	5,730	8,201	12,573	15,409
9,900	4,669	5,147	6,599	10,260	14,619	15,951
10,350	4,970	5,688	7,952	12,347	15,723	16,426
10,800	5,280	6,435	9,548	14,252	16,210	16,825
11,250	5,712	7,341	11,369	15,578	16,681	17,187
11,900	6,204	8,521	13,171	16,259	17,112	17,603
12,150	6,772	9,760	14,510	16,757	17,520	18,383
12,600	7,564	11,155	15,783	17,095	17,908	19,265
13,050	8,498	12,789	16,600	17,637	18,527	20,573
13,500	9,452	14,267	17,170	18,163	19,205	22,421
13,750	10,623	15,508	18,181	18,551	20,172	24,979

Table 2. Stagnation heating factors.

Mach	K_1	K_2
1	1.00	1.00
5	1.16	1.20
10	1.14	1.18
15	1.16	1.16
20	1.23	1.16
25	1.40	1.25
30	1.45	1.26

Table 3. Turbulent flow correction factors, $A_1 \times 10^{-4}$.

	Wedge or cone angle ± angle of attack, deg								
M_∞	−10	−5	−1	0	+1	+5	+10	+20	+40
2	0.780	0.850	0.960	0.960	1.20	1.30	1.50	1.60	1.70
3	1.39	1.50	1.66	1.50	1.66	1.78	1.91	2.19	2.30
5	1.20	1.65	2.20	1.70	1.91	2.16	2.41	2.65	2.68
10	1.10	1.53	2.30	2.00	2.41	3.07	3.75	4.44	4.51
15	0.920	1.45	2.40	2.00	2.56	3.67	4.79	6.08	6.26
20	0.690	1.30	2.13	2.00	2.65	4.13	5.62	9.19	8.77
25	0.538	0.914	1.88	1.80	2.65	4.20	6.0	8.5	8.0
30	0.436	0.763	1.74	1.70	2.65	4.5	6.0	6.0	6.0

Table 4. Laminar flow correction factors, $A_2 \times 10^{-4}$.

	Wedge or cone angle ± angle of attack, deg								
M_∞	−10	−5	−1	0	+1	+5	+10	+20	+40
2	0.300	0.310	0.320	0.290	0.300	0.310	0.330	0.340	0.350
3	0.400	0.416	0.437	0.400	0.433	0.448	0.460	0.457	0.460
5	0.600	0.655	0.714	0.625	0.728	0.779	0.826	0.855	0.671
10	0.817	0.970	1.24	1.20	1.33	1.52	1.66	1.70	1.53
15	0.930	1.25	1.80	1.50	1.88	2.20	2.41	2.43	2.05
20	0.960	1.45	2.03	2.06	2.38	2.90	3.13	3.07	2.62
25	0.914	1.43	2.25	2.03	2.73	3.40	3.50	3.00	2.55
30	0.844	1.40	2.42	1.89	3.00	3.50	3.50	2.00	2.00

Table 5. Transition Reynolds numbers and transition Mach number coefficients.

(a) Conical flow.

α, deg	log Re_T	C_m	
		Sharp leading edge	Blunt leading edge
0–7	5.3	0.25	0.20
7–20	5.3	0.20	0.18
20–40	5.3	0.15	0.12

(b) Two dimensional flow.

		C_m					
		Sharp leading edge			Blunt leading edge		
Λ, deg	log Re_T	$\alpha \leq 7°$	$7° < \alpha < 20°$	$\alpha \geq 20°$	$\alpha \leq 7°$	$7° < \alpha < 20°$	$\alpha \geq 20°$
0–45	5.3	0.23	0.20	0.18	0.20	0.18	0.15
45–60	5.3	0.20	0.18	0.15	0.18	0.15	0.12
60–75	5.3	0.17	0.15	0.13	0.15	0.13	0.11

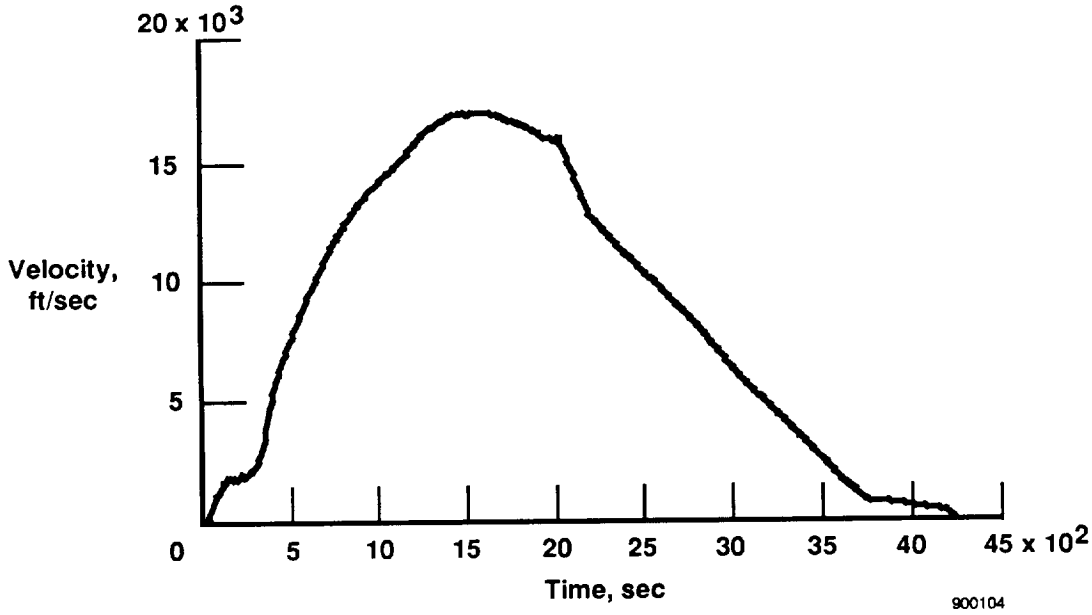

(a) Velocity.

Figure 1. Time history of flight simulation parameters.

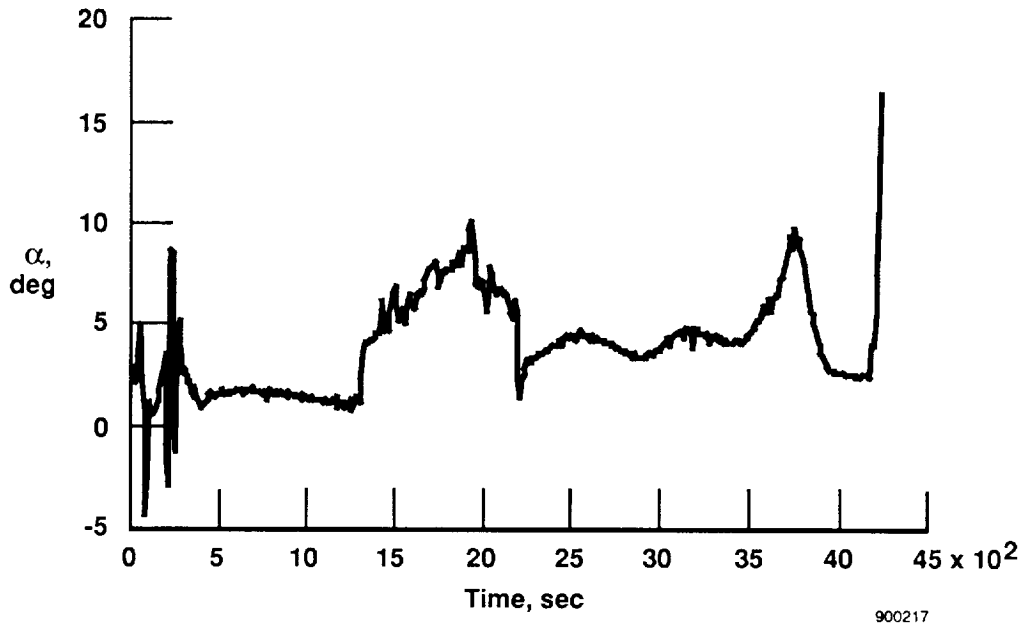

(b) Angle of attack.

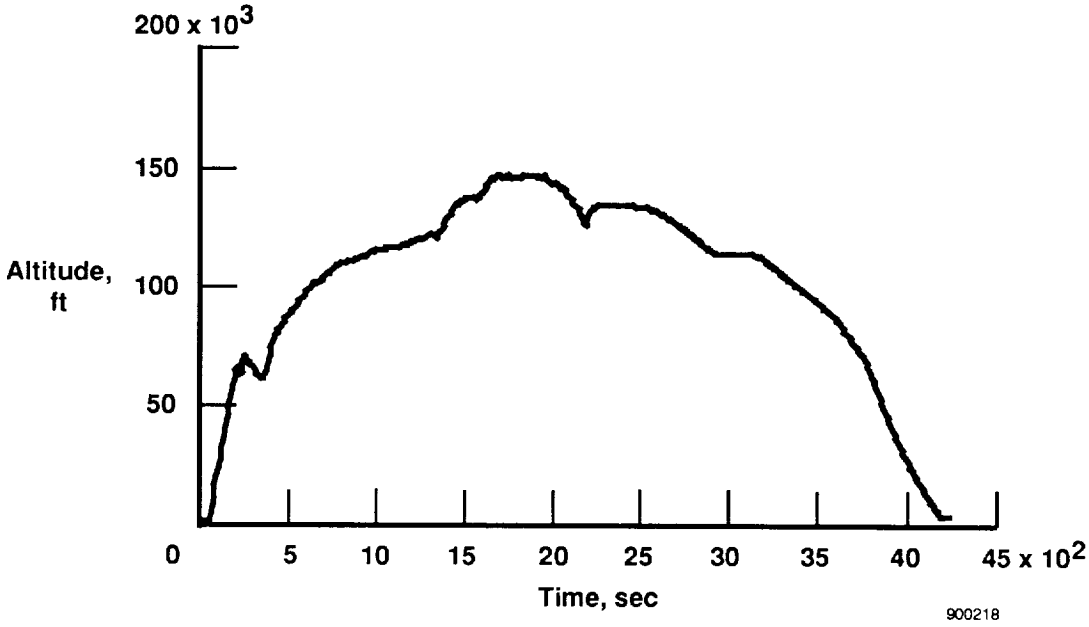

(c) Altitude.

Figure 1. Concluded.

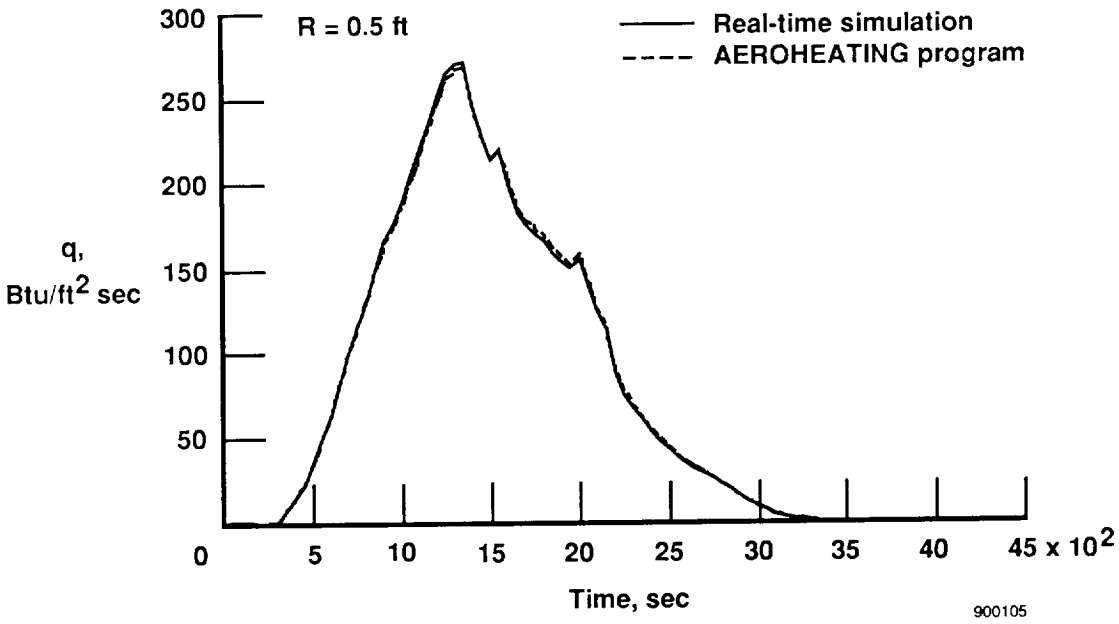

(a) Three-dimensional surface heating rates.

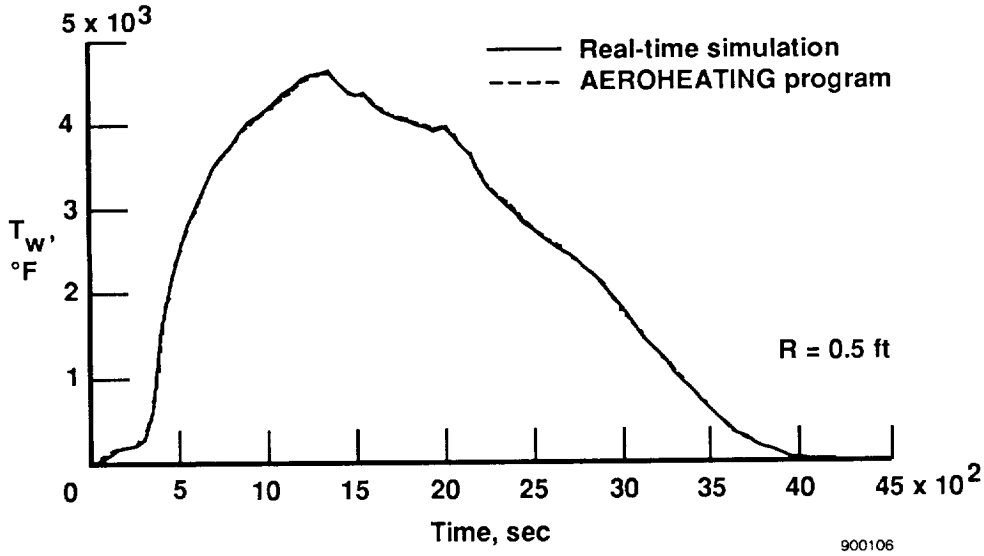

(b) Three-dimensional surface temperatures.

Figure 2. Stagnation heating rates and temperatures from the real-time simulation compared with values calculated by the AEROHEATING program.

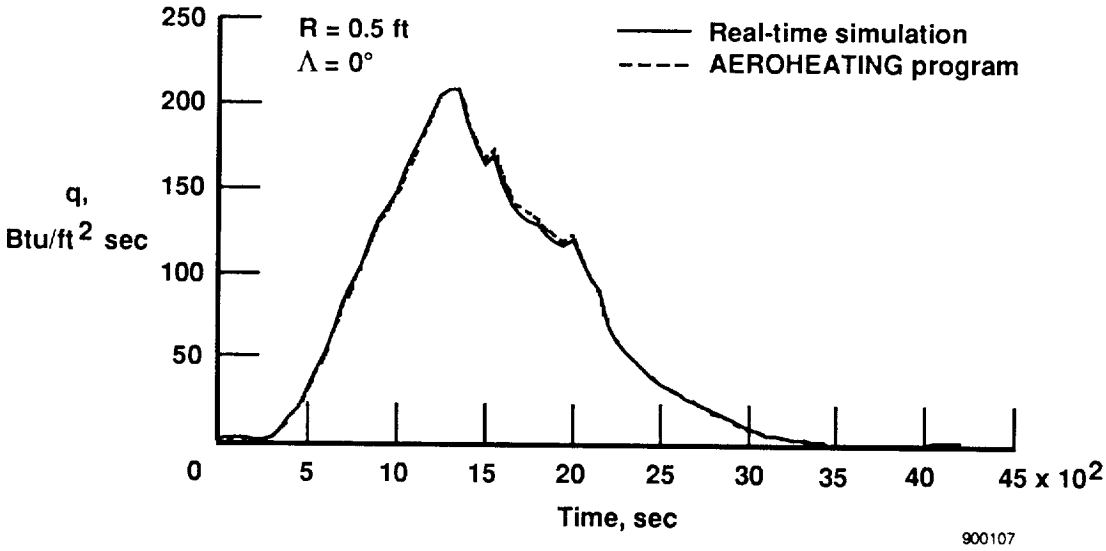

(c) Two-dimensional surface heating rates with a 0°-leading-edge sweep.

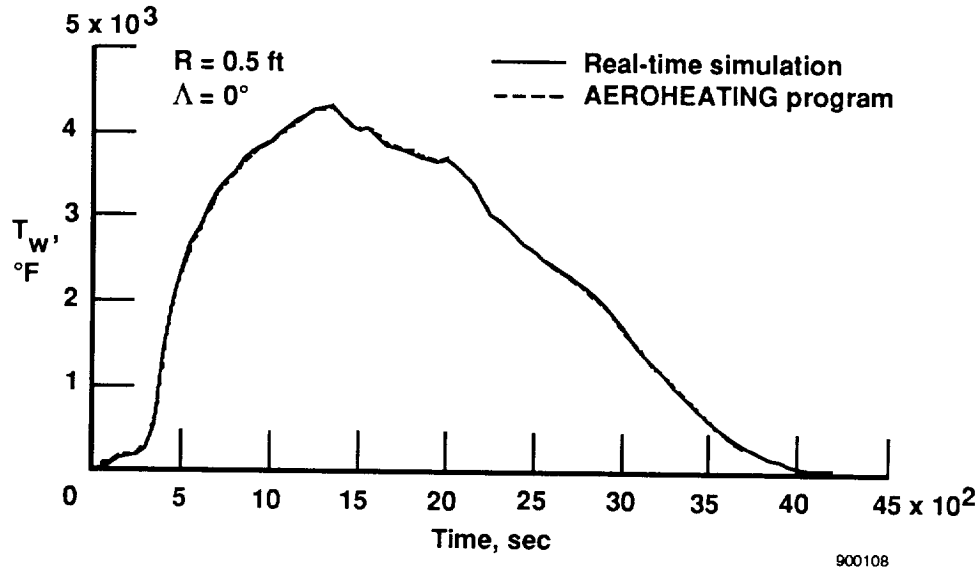

(d) Two-dimensional surface temperatures with a 0°-leading-edge sweep.

Figure 2. Continued.

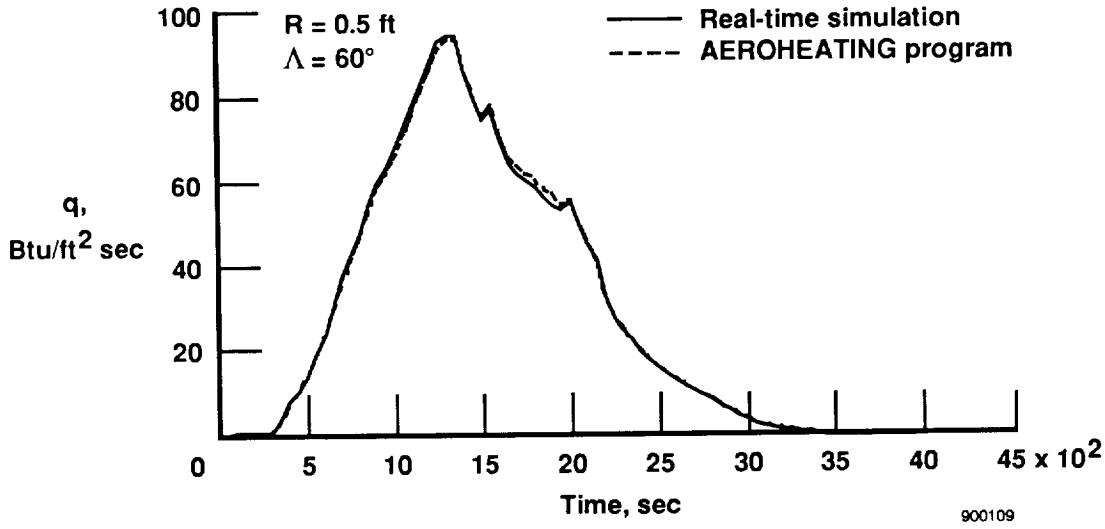

(e) Two-dimensional surface heating rates with a 60°-leading-edge sweep.

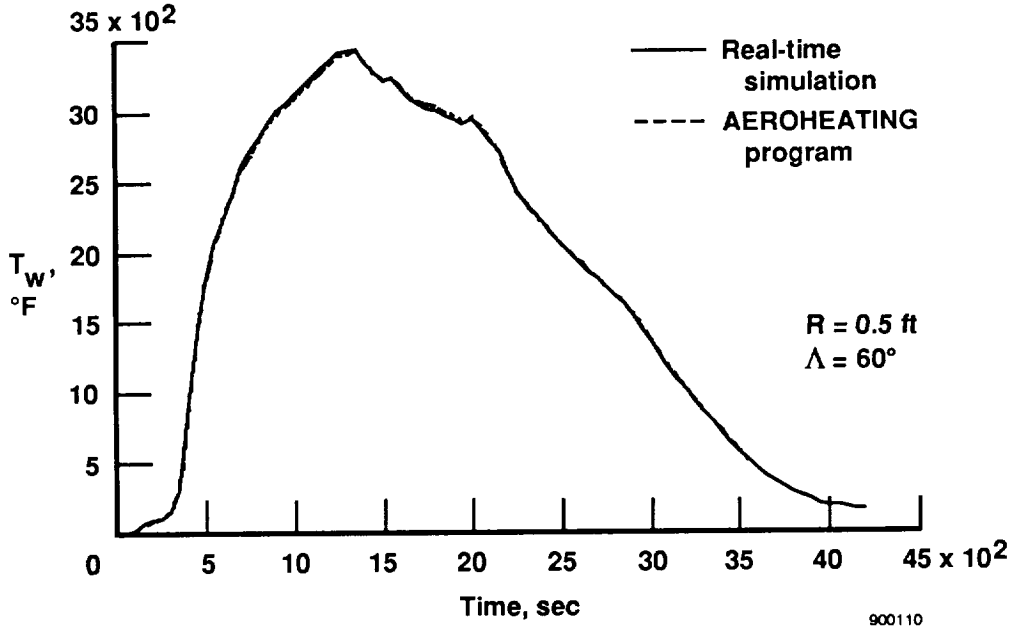

(f) Two-dimensional surface temperatures with a 60°-leading-edge sweep.

Figure 2. Concluded.

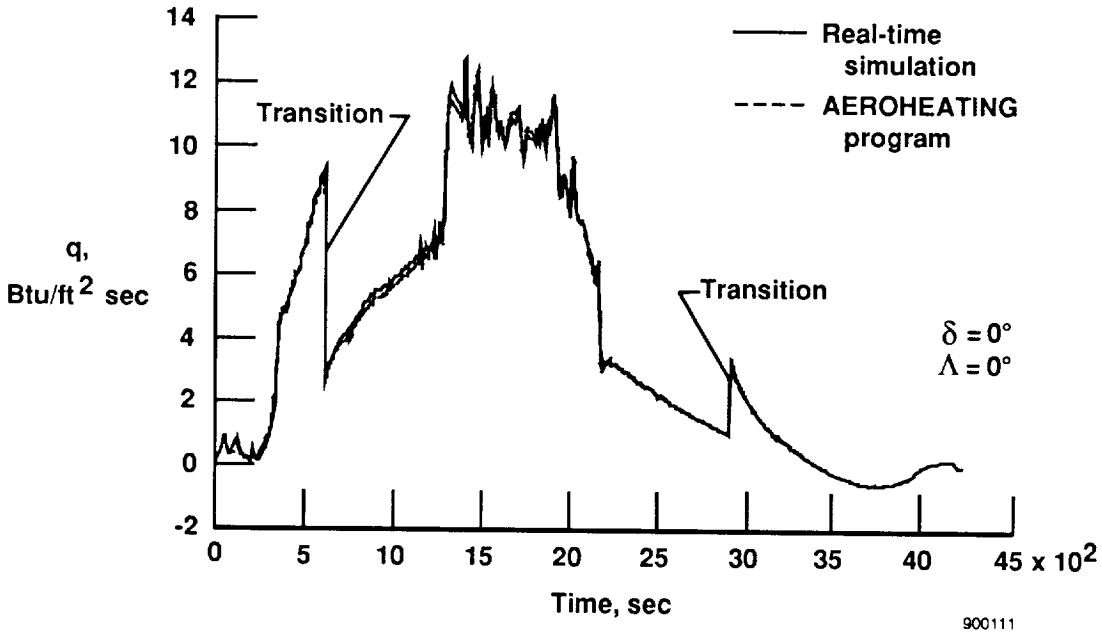

(a) Lower surface heating rates, $x = 3$ ft.

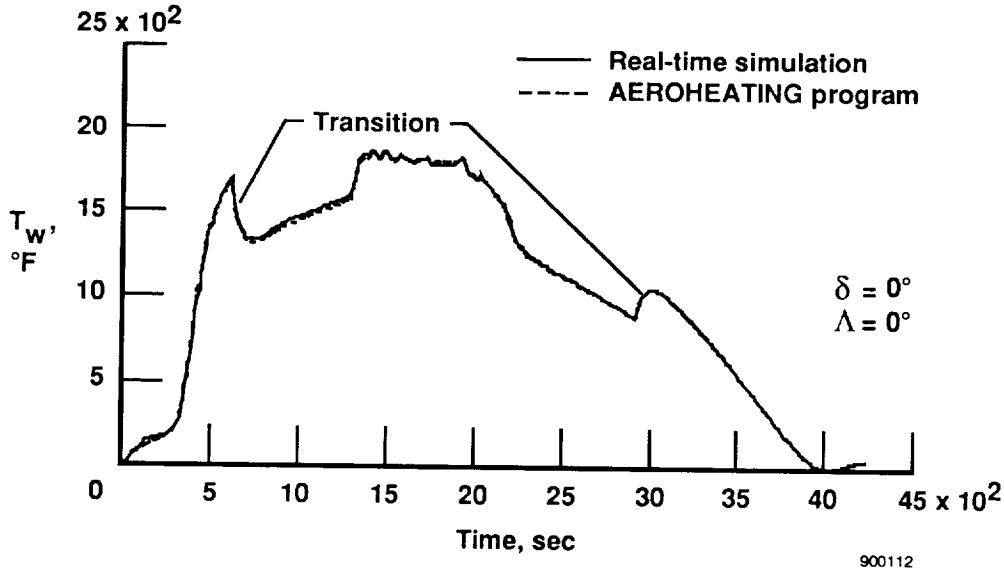

(b) Lower surface temperatures, $x = 3$ ft.

Figure 3. Heating rates and temperatures from the real-time simulation compared with values calculated by the AEROHEATING program for a zero pressure gradient surface.

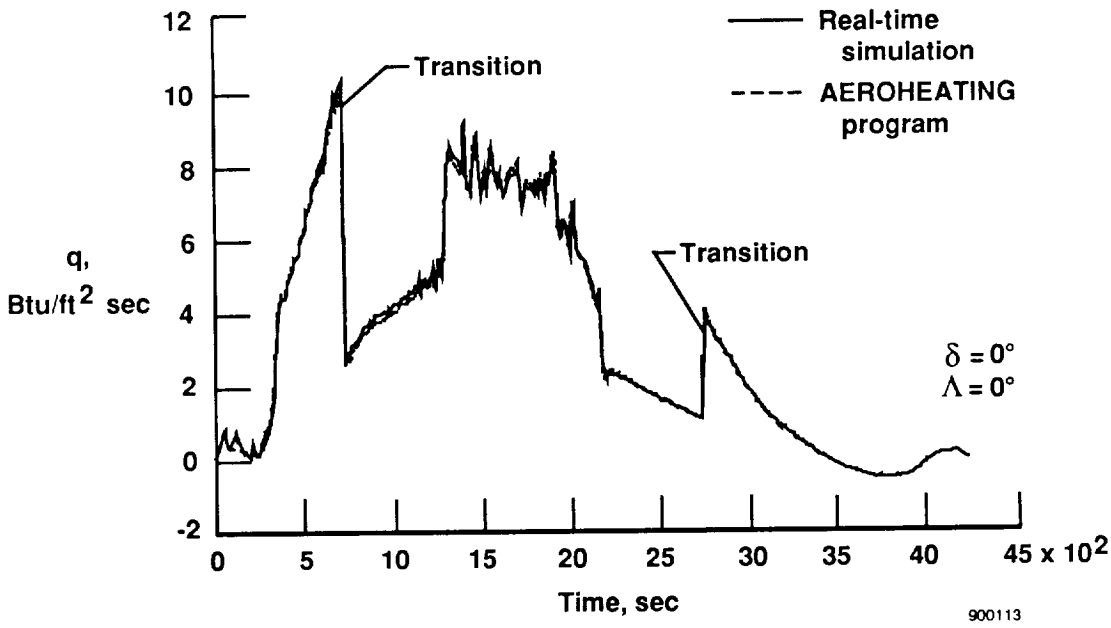

(c) Lower surface heating rates, x = 6 ft.

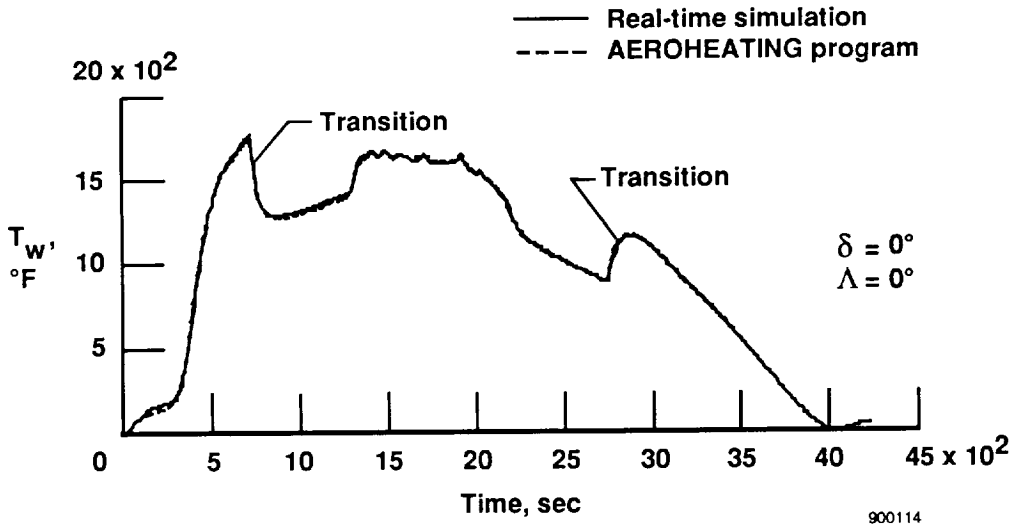

(d) Lower surface temperatures, x = 6 ft.

Figure 3. Continued.

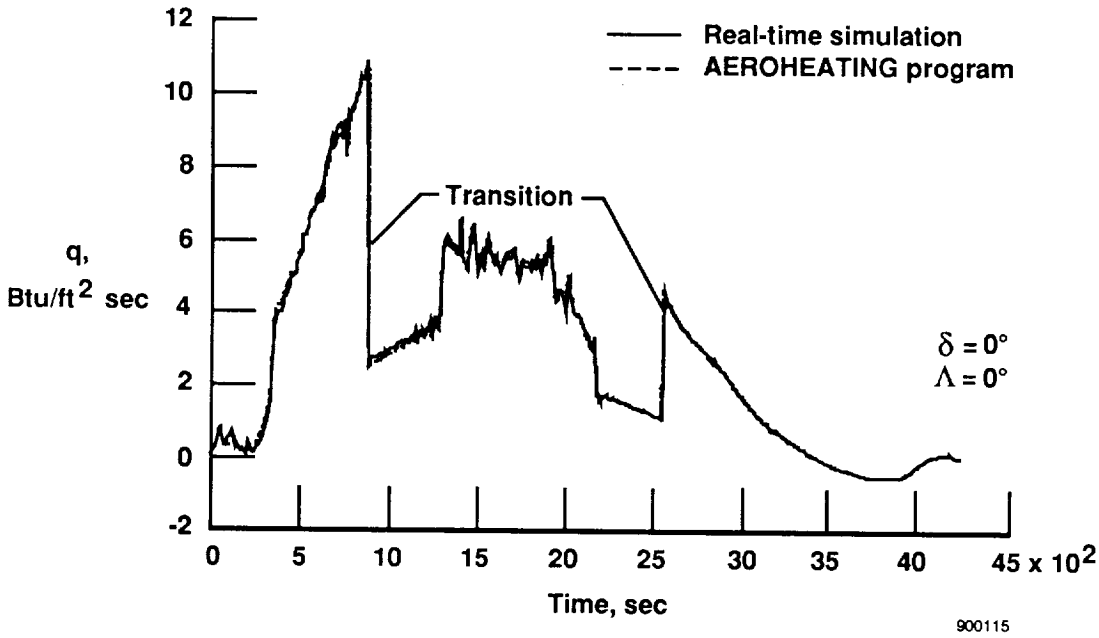

(c) Lower surface heating rates, $x = 12$ ft.

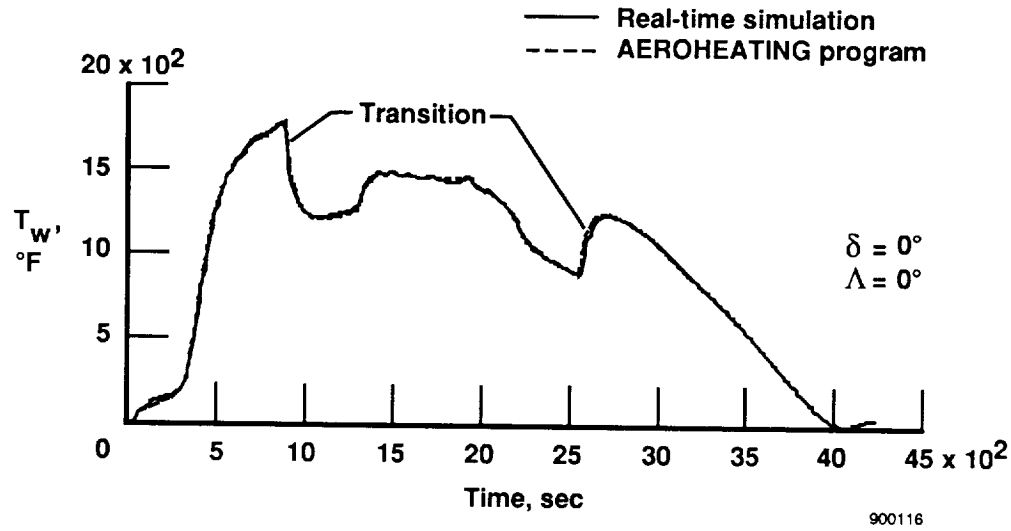

(f) Lower surface temperatures, $x = 12$ ft.

Figure 3. Continued.

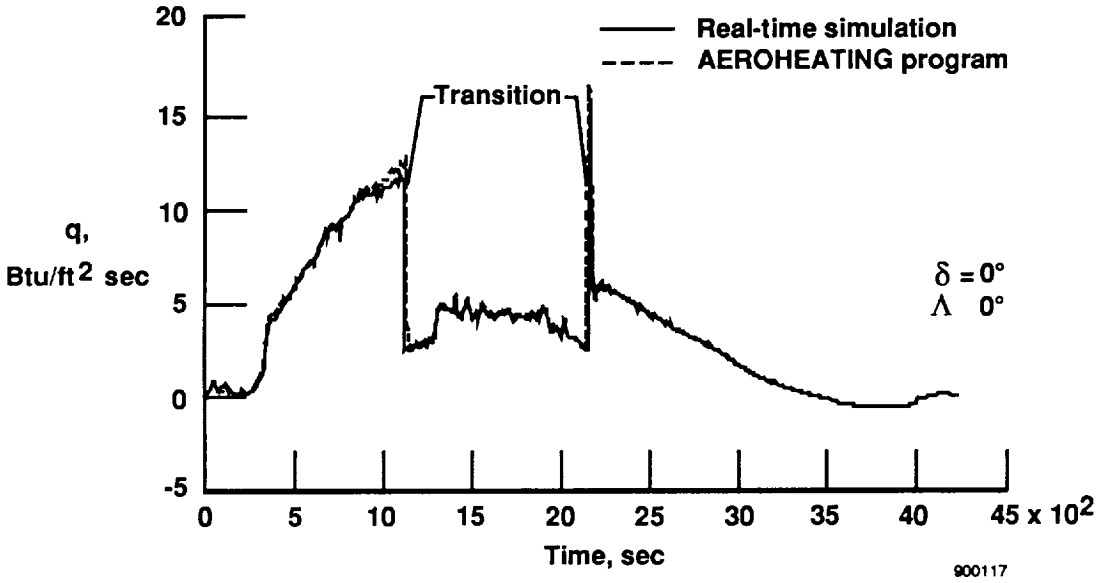

(g) Lower surface heating rates, x = 24 ft.

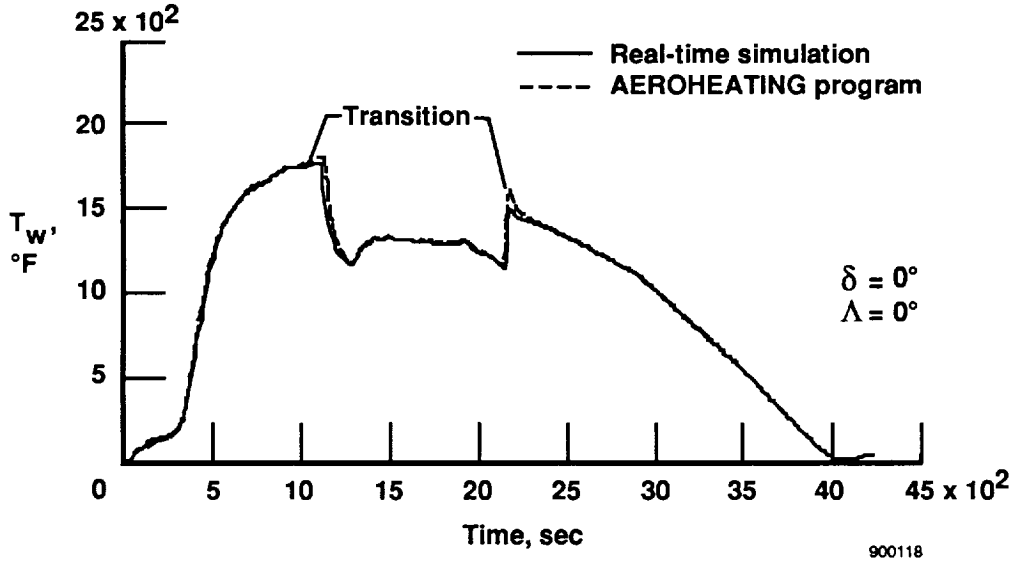

(h) Lower surface temperatures, x = 24 ft.

Figure 3. Continued.

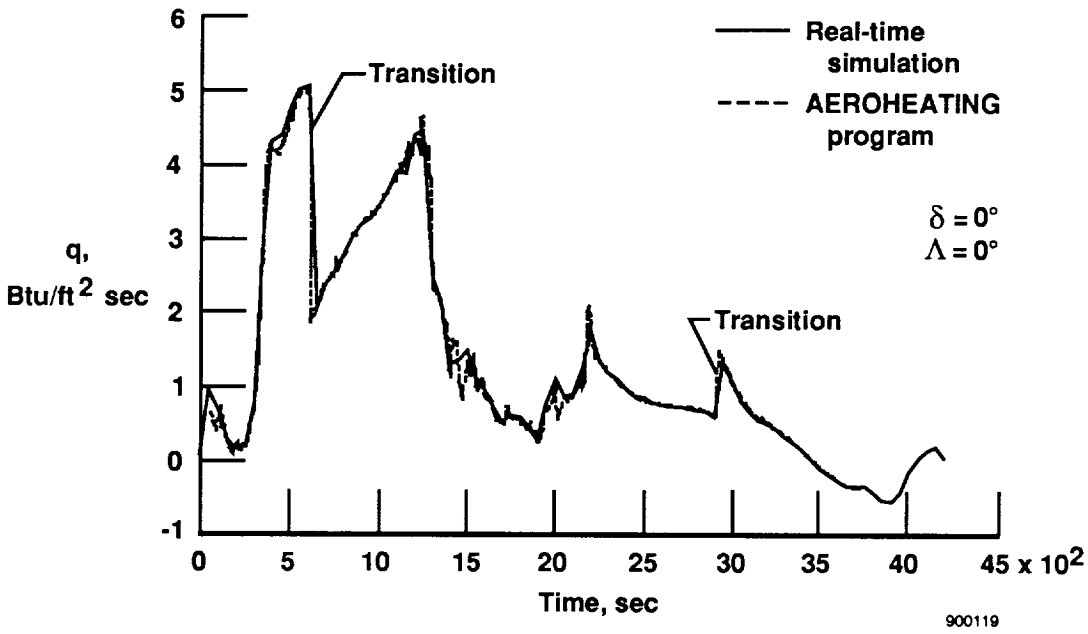

(i) Upper surface heating rates, $x = 3$ ft.

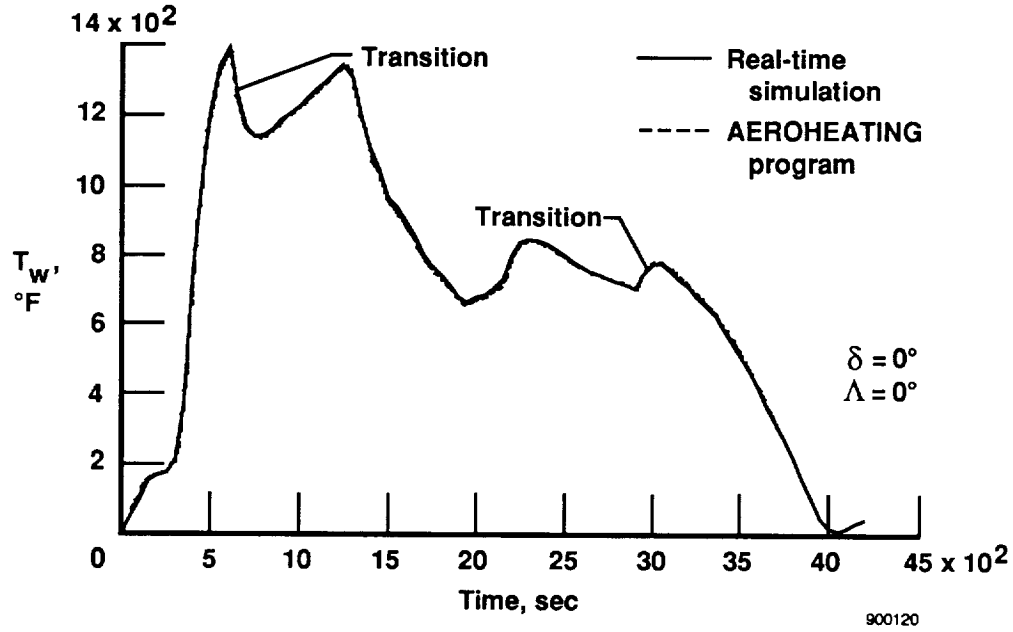

(j) Upper surface temperatures, $x = 3$ ft.

Figure 3. Continued.

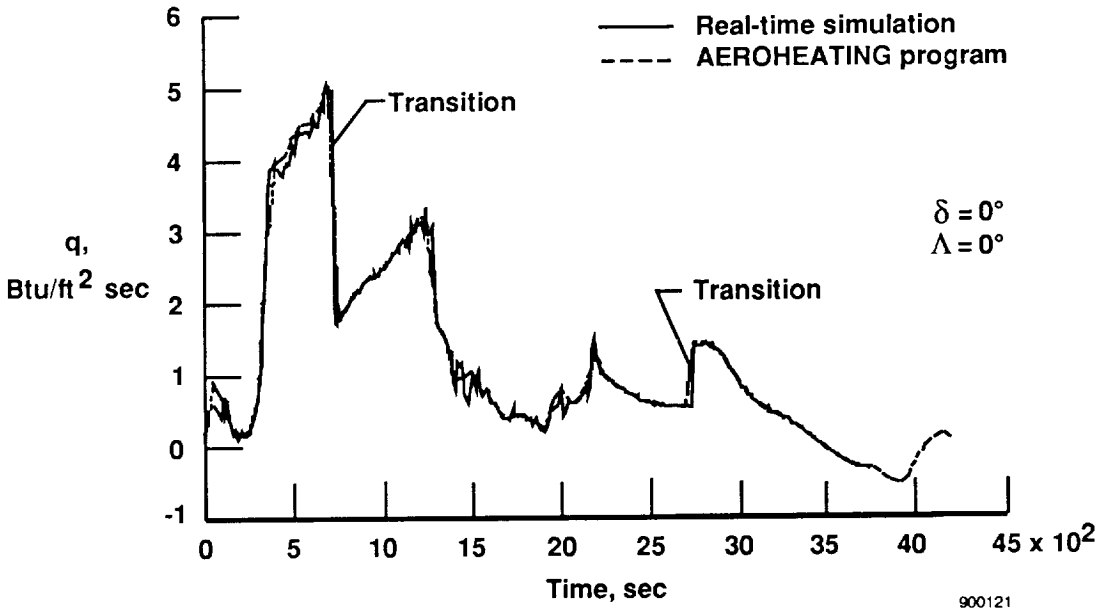

(k) Upper surface heating rates, $x = 6$ ft.

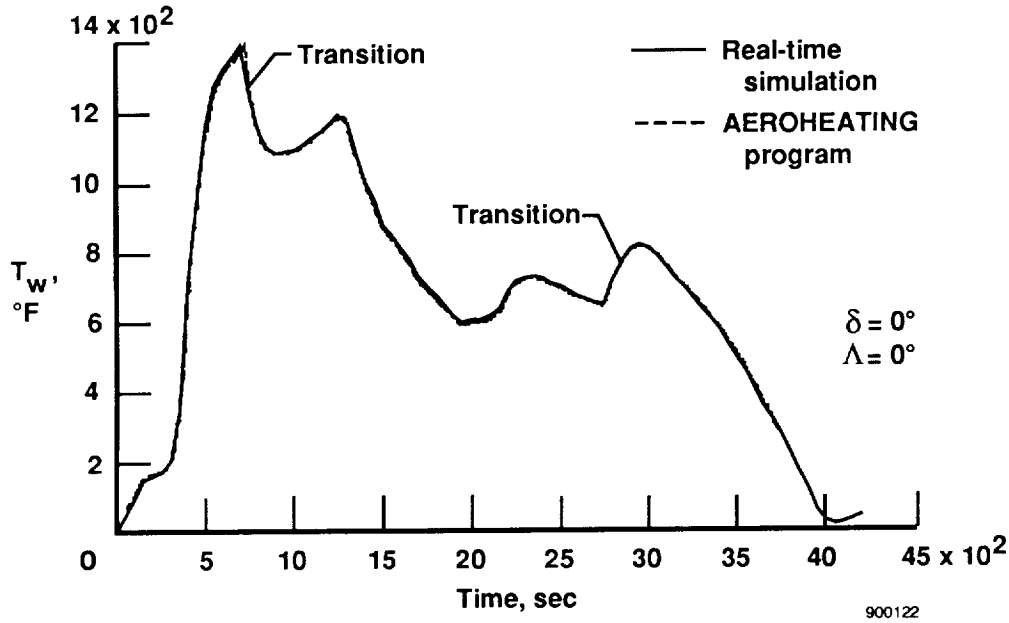

(l) Upper surface temperatures, $x = 6$ ft.

Figure 3. Continued.

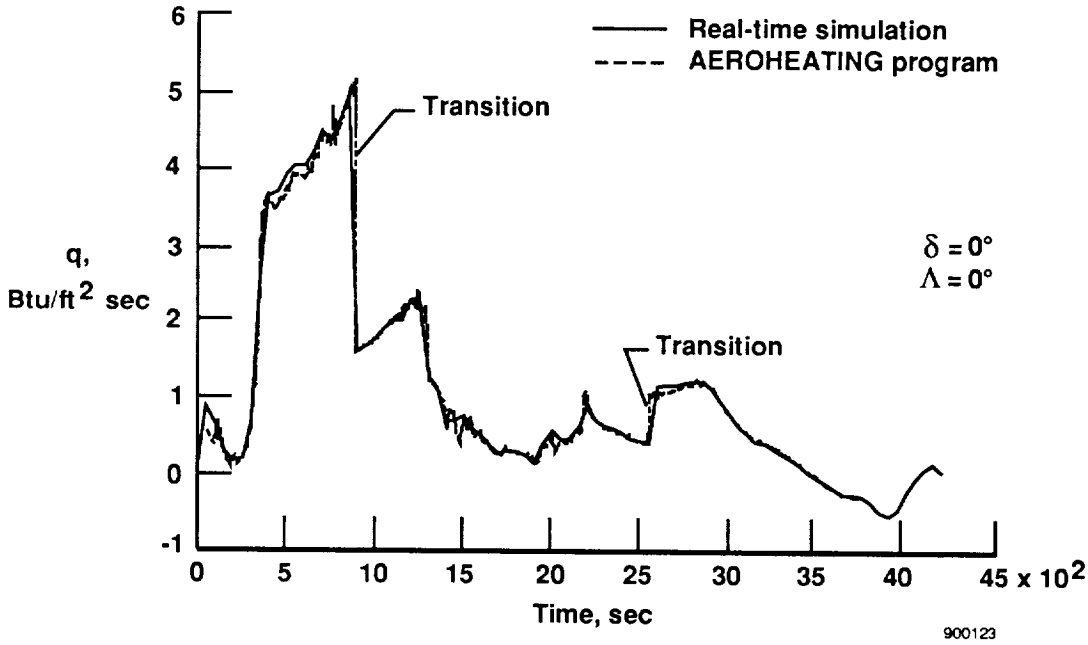

(m) Upper surface heating rates, x = 12 ft.

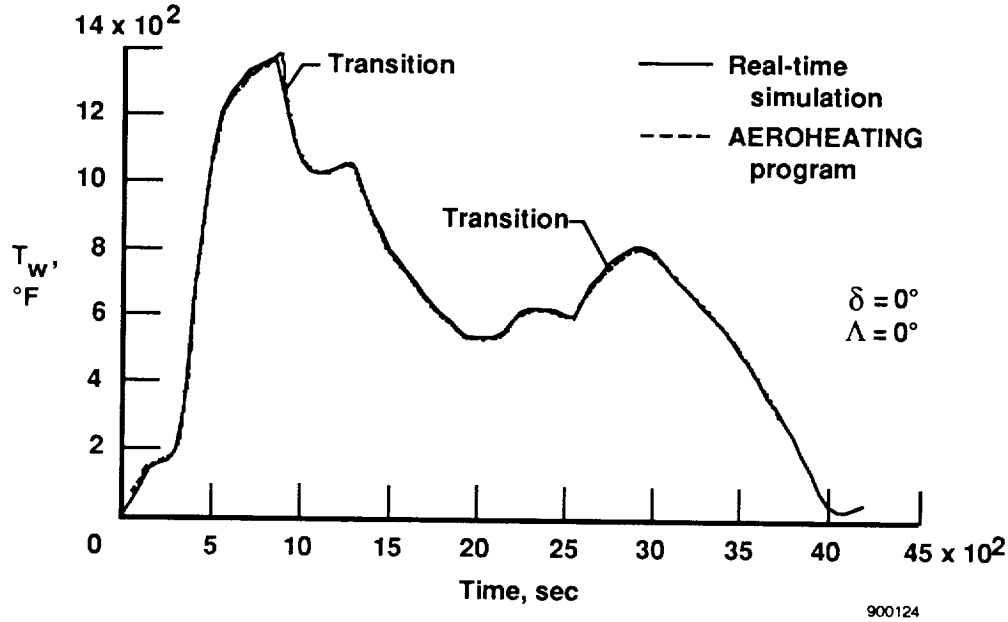

(n) Upper surface temperatures, x = 12 ft.

Figure 3. Continued.

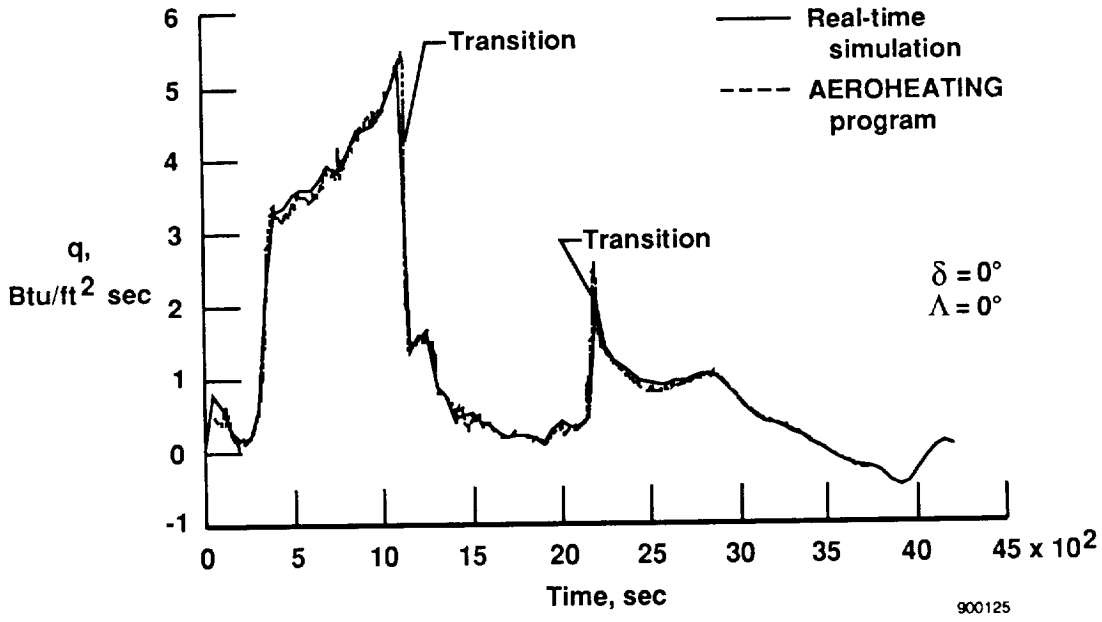

(o) Upper surface heating rates, x = 24 ft.

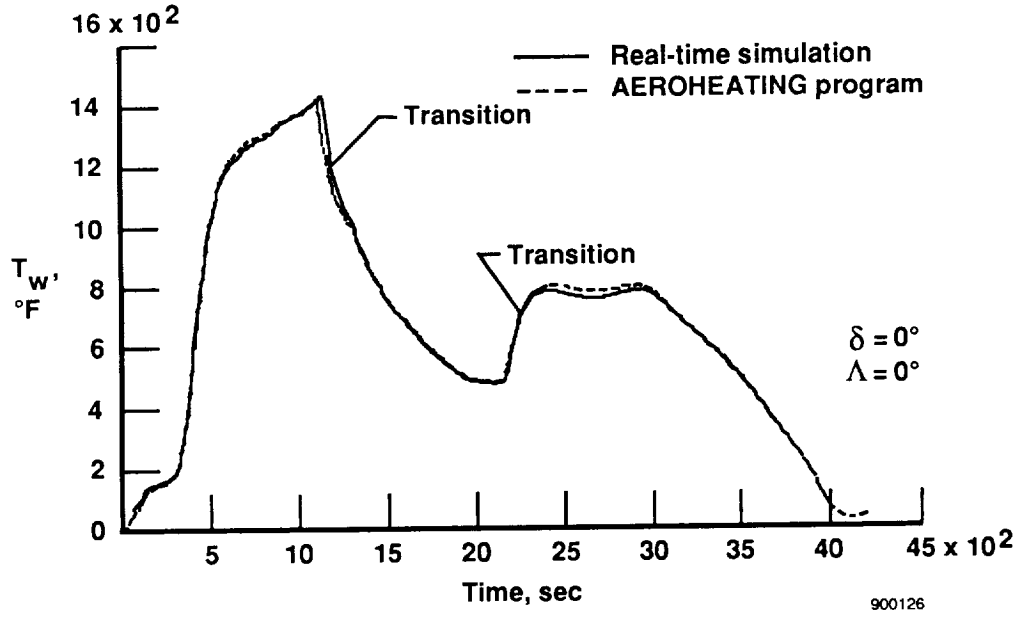

(p) Upper surface temperatures, x = 24 ft.

Figure 3. Concluded.

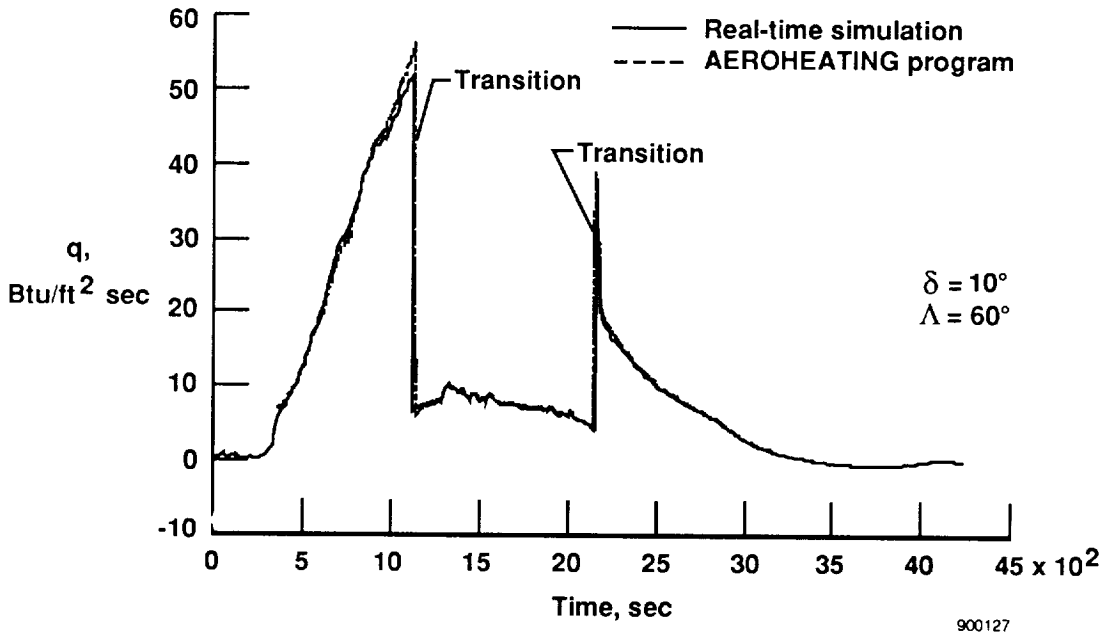

(a) Lower surface heating rates, x = 3 ft.

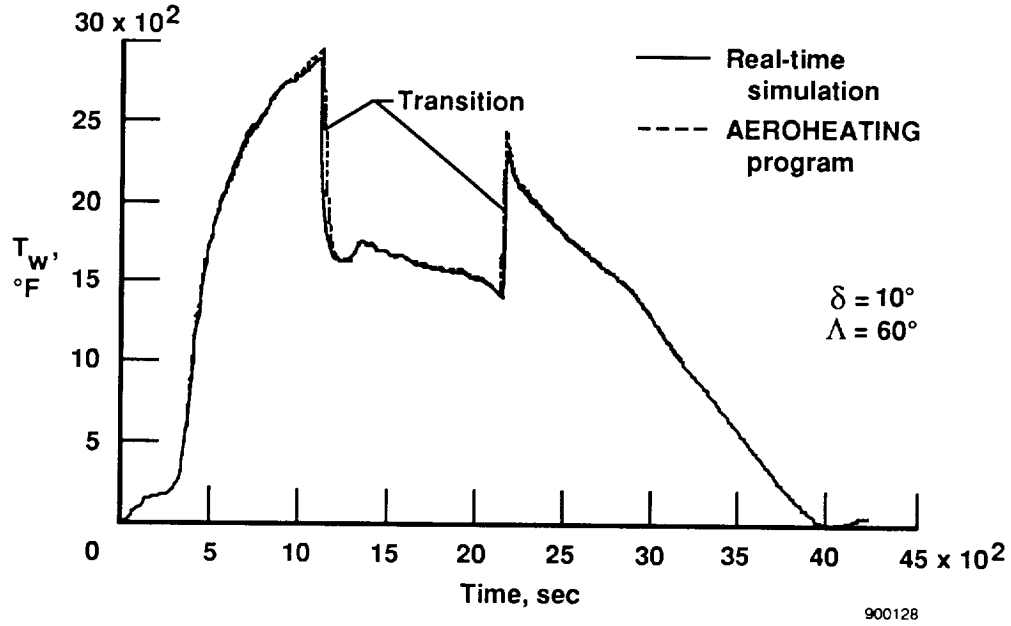

(b) Lower surface temperatures, x = 3 ft.

Figure 4. Heating rates and temperatures from the real-time simulation compared with values calculated by the AEROHEATING program for a zero pressure gradient surface with a 60°-leading-edge sweep.

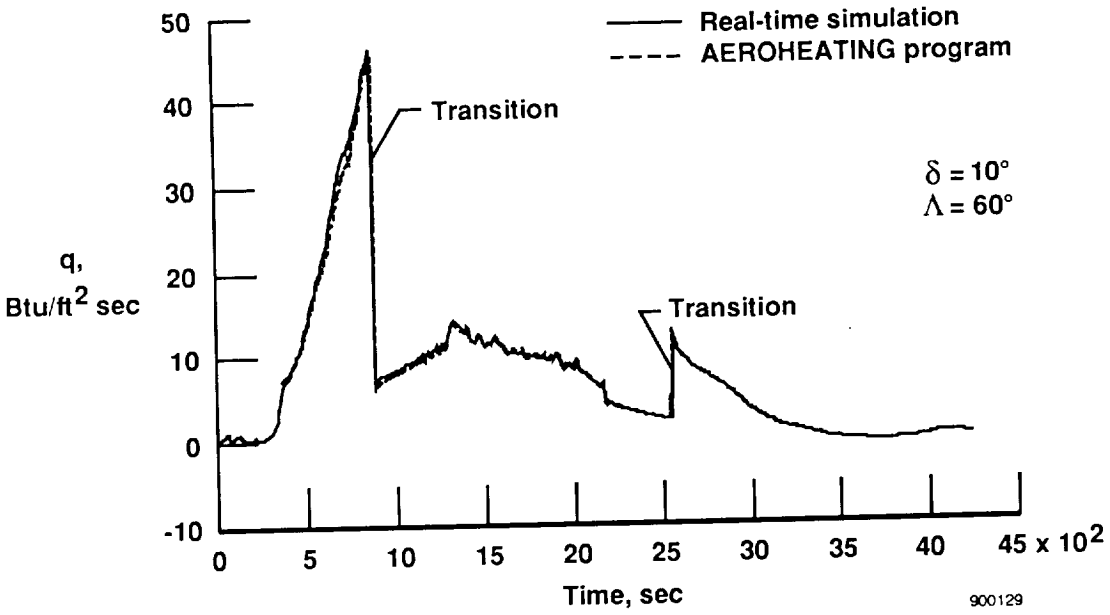

(c) Lower surface heating rates, $x = 6$ ft.

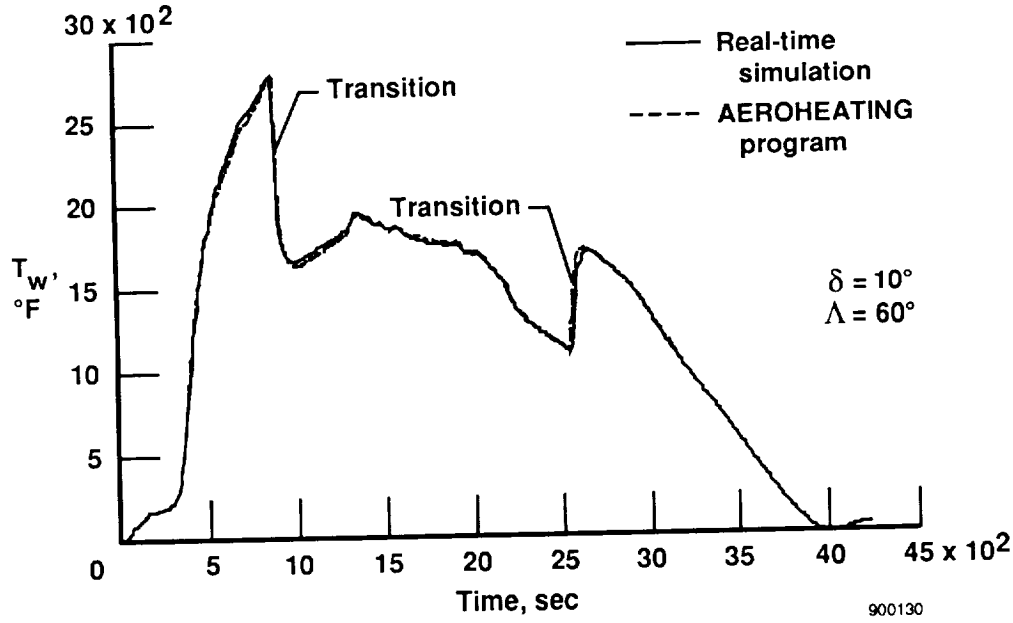

(d) Lower surface temperatures, $x = 6$ ft.

Figure 4. Continued.

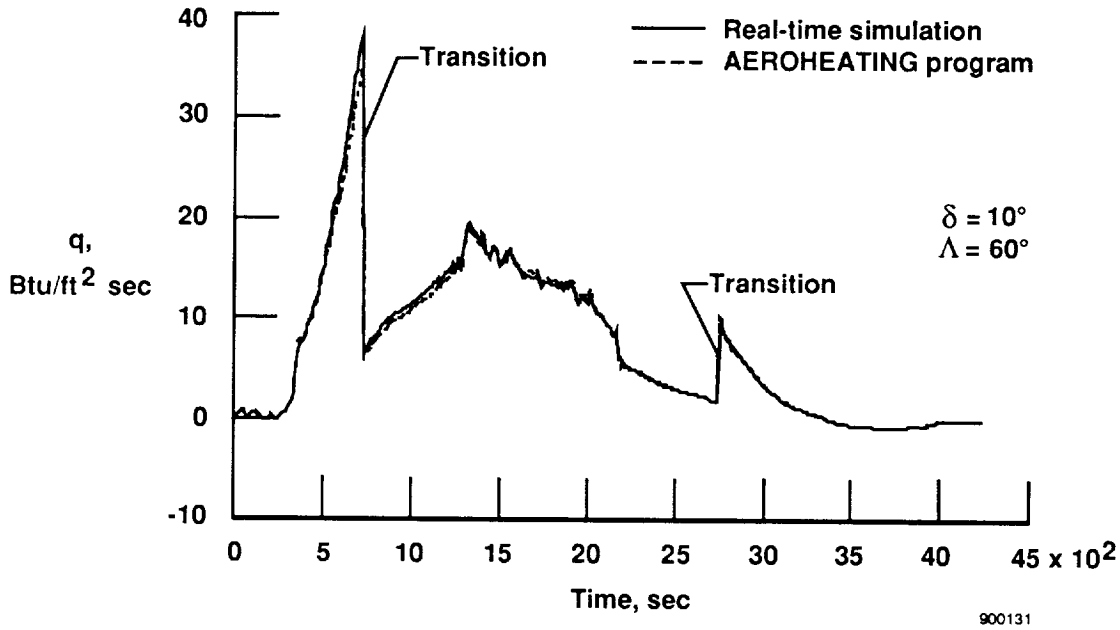

(e) Lower surface heating rates, x = 12 ft.

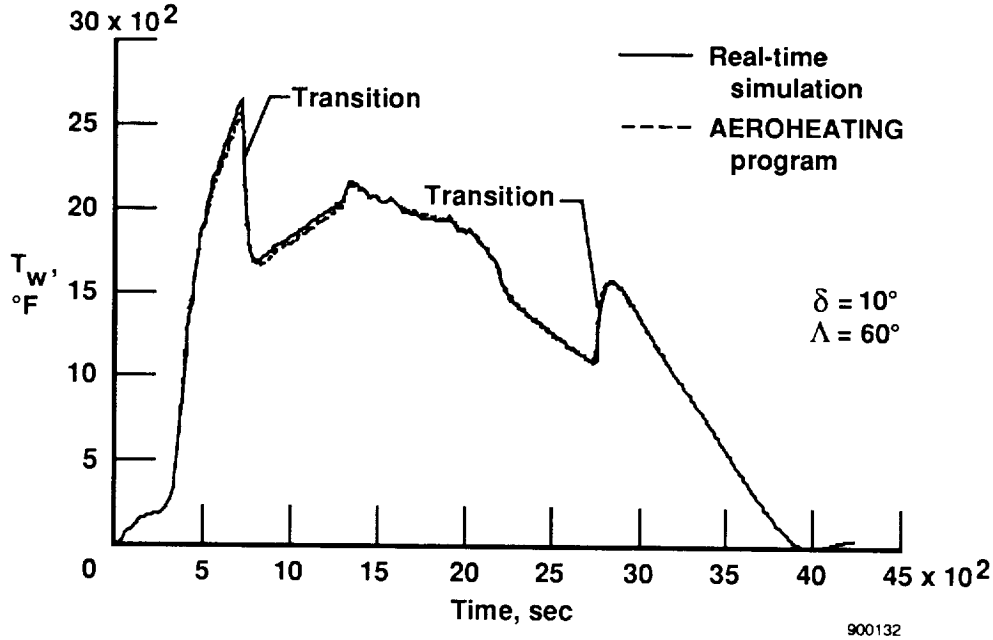

(f) Lower surface temperatures, x = 12 ft.

Figure 4. Continued.

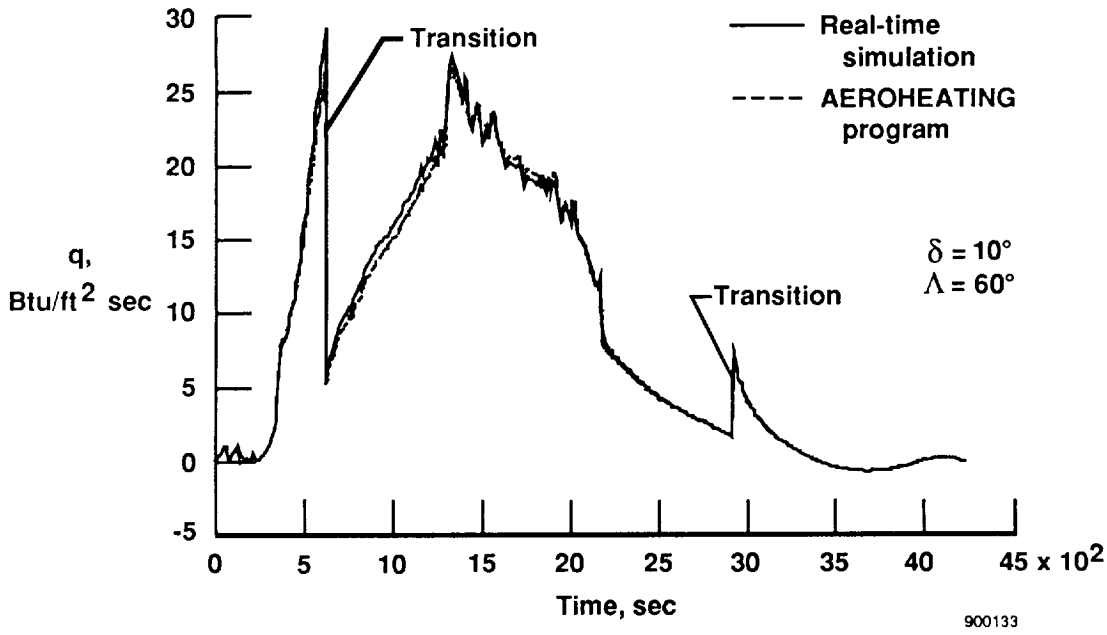

(g) Lower surface heating rates, $x = 24$ ft.

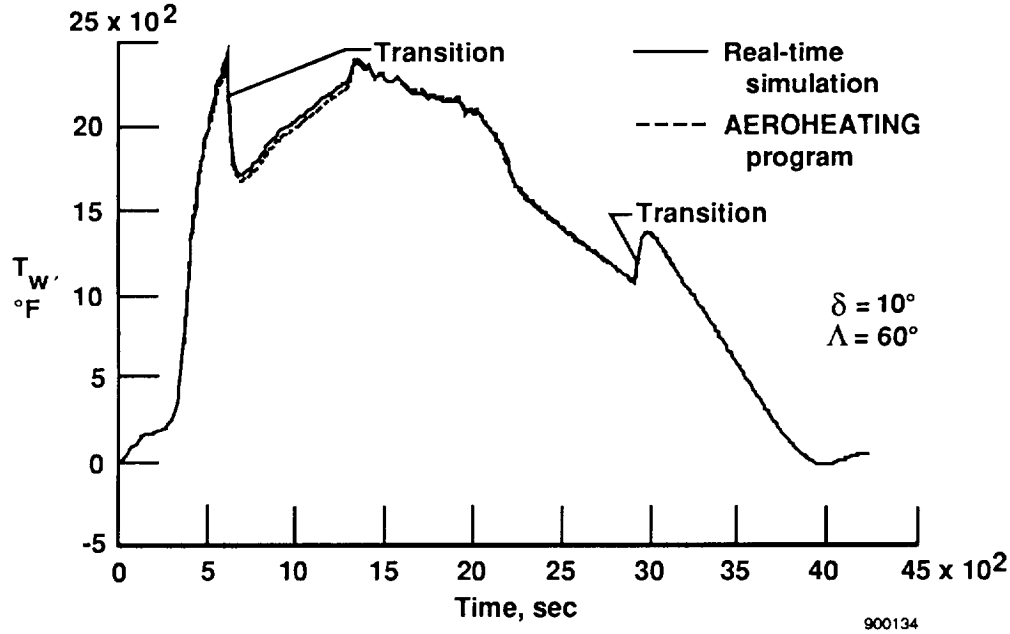

(h) Lower surface temperatures, $x = 24$ ft.

Figure 4. Continued.

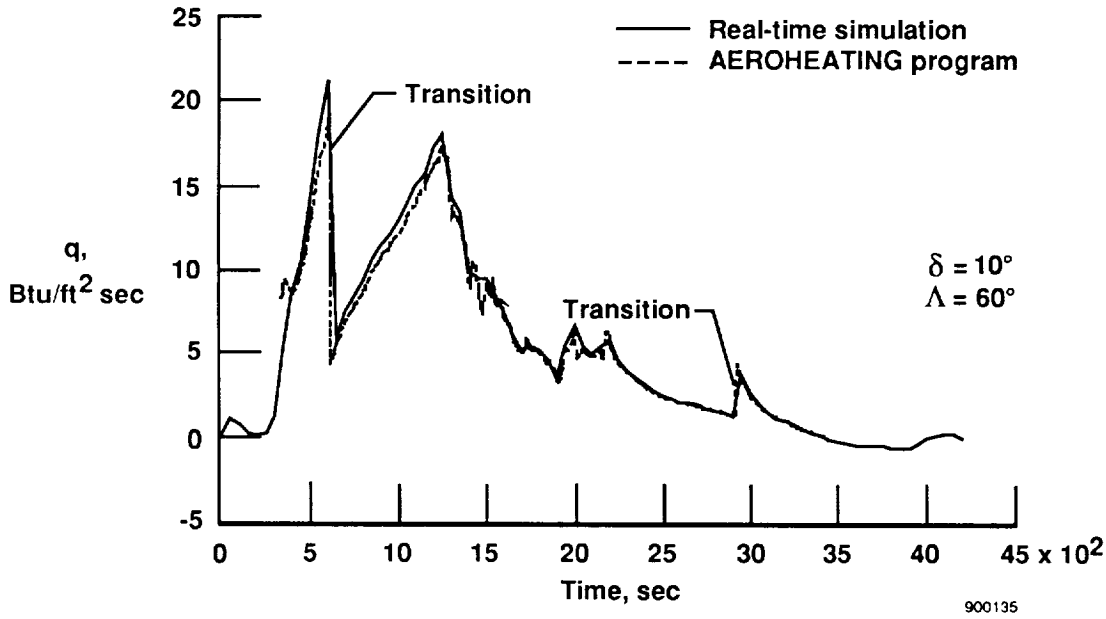

(i) Upper surface heating rates, x = 3 ft.

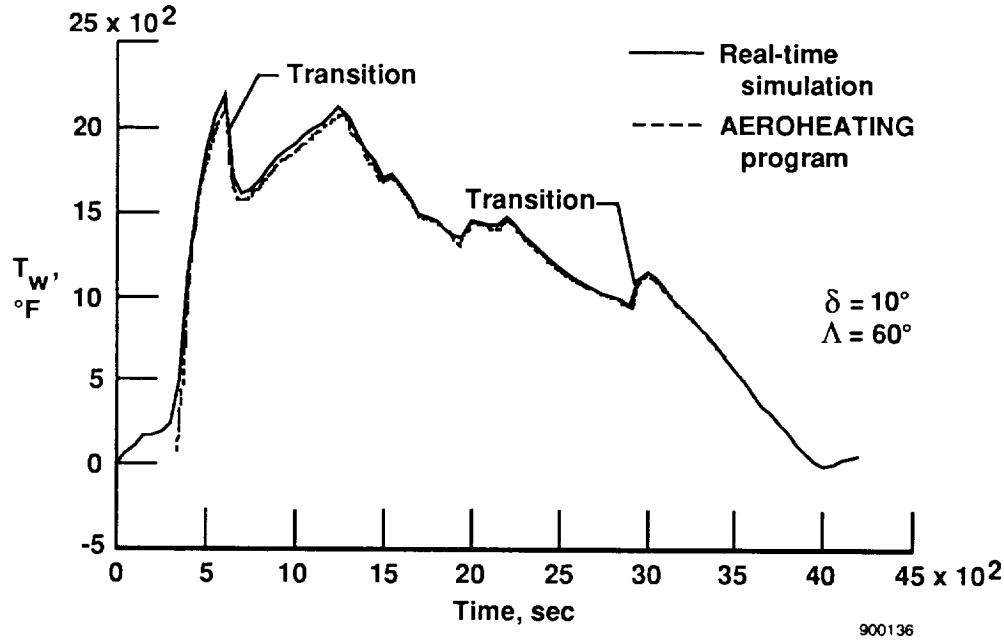

(j) Upper surface temperatures, x = 3 ft.

Figure 4. Continued.

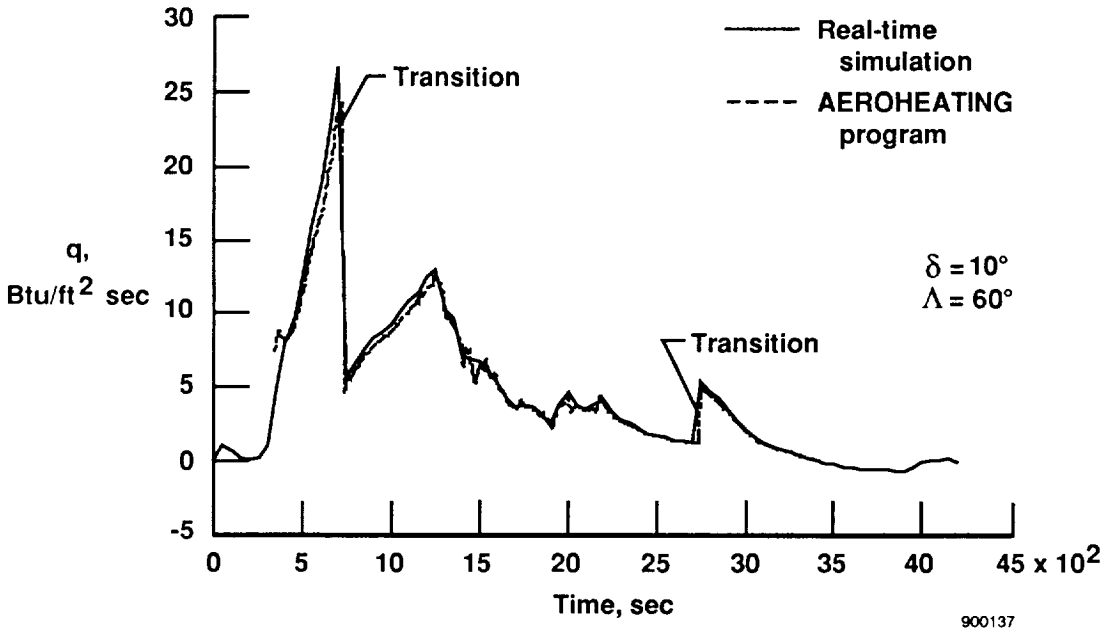

(k) Upper surface heating rates, $x = 6$ ft.

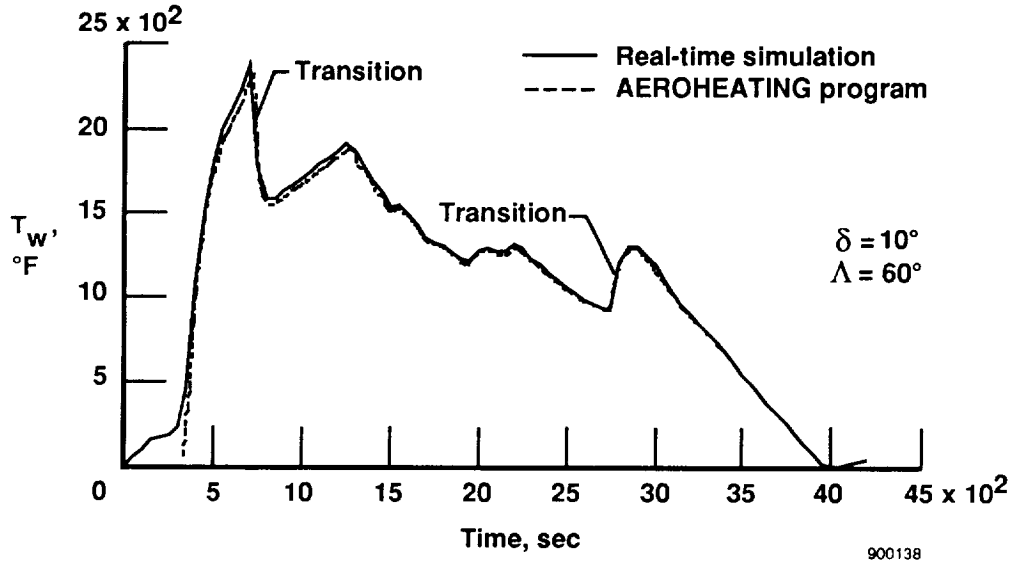

(l) Upper surface temperatures, $x = 6$ ft.

Figure 4. Continued.

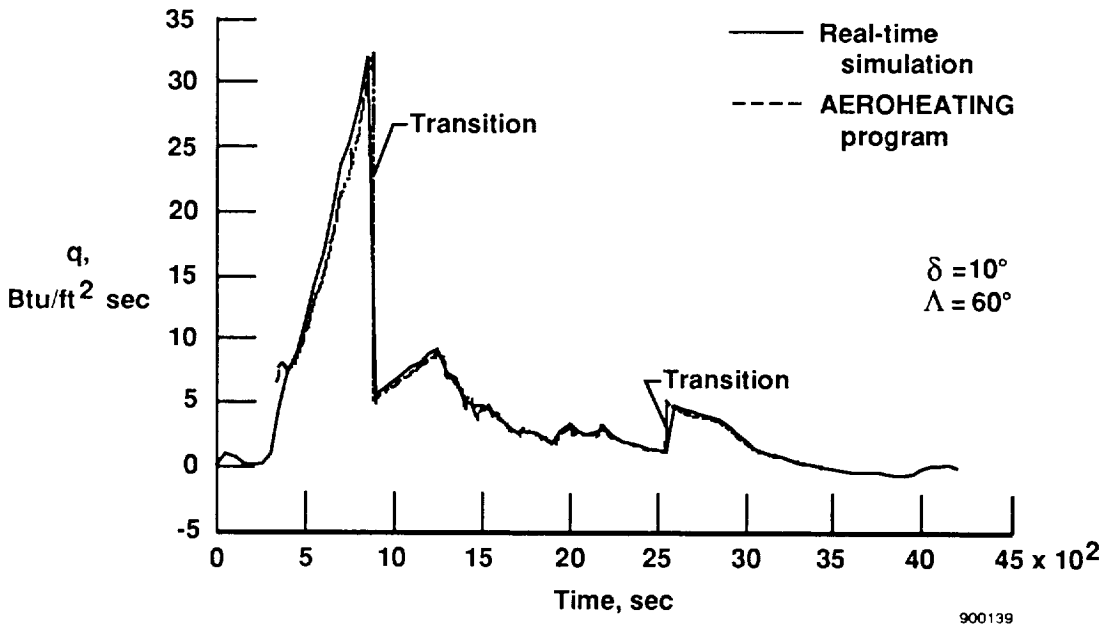

(m) Upper surface heating rates, x = 12 ft.

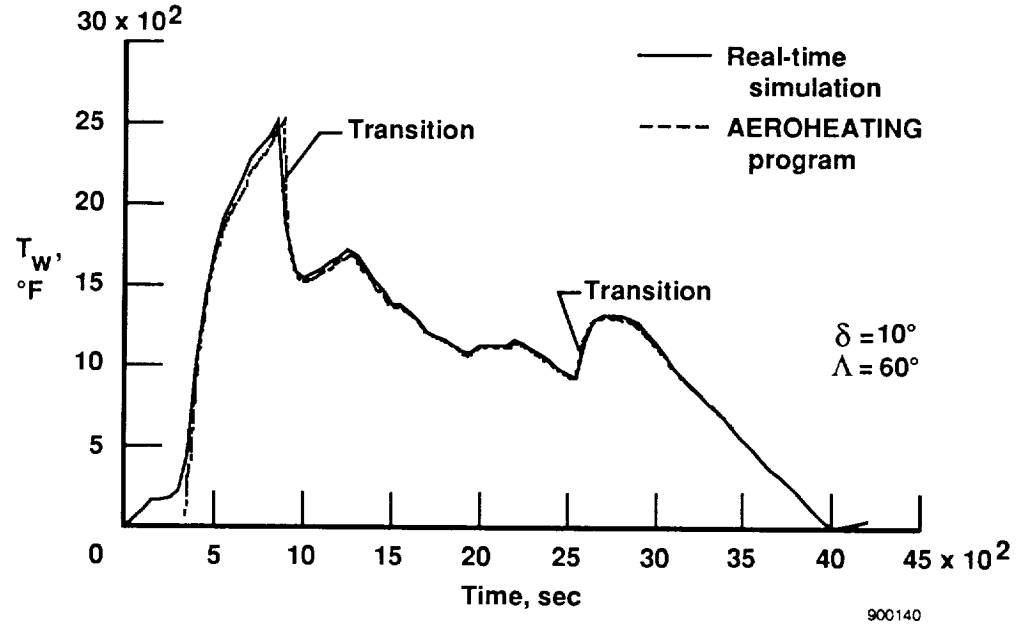

(n) Upper surface temperatures, x = 12 ft.

Figure 4. Continued.

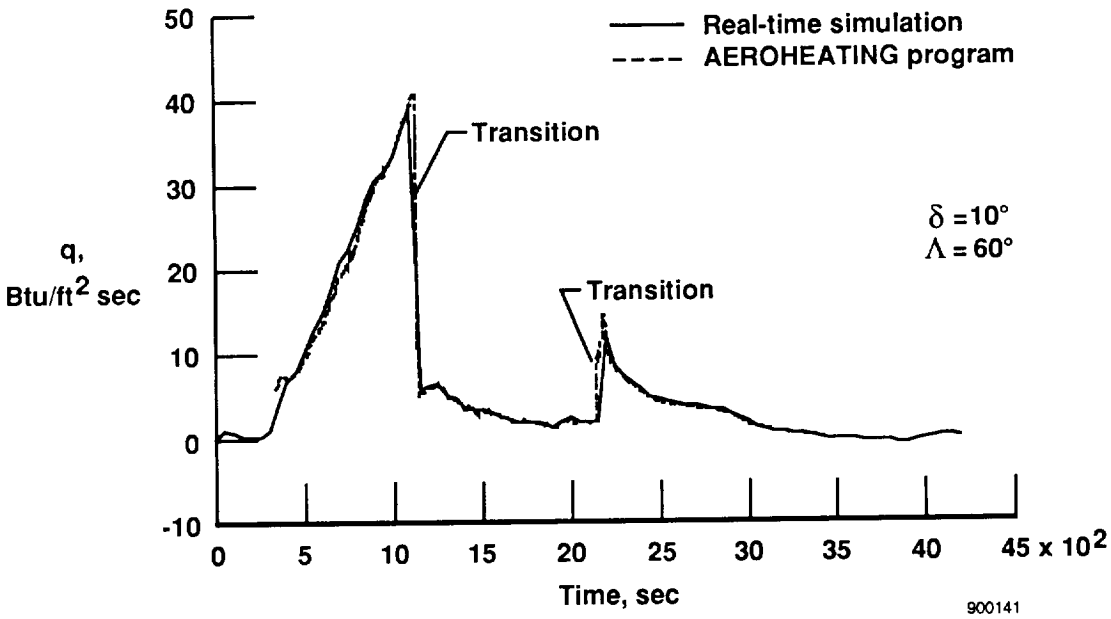

(o) Upper surface heating rates, $x = 24$ ft.

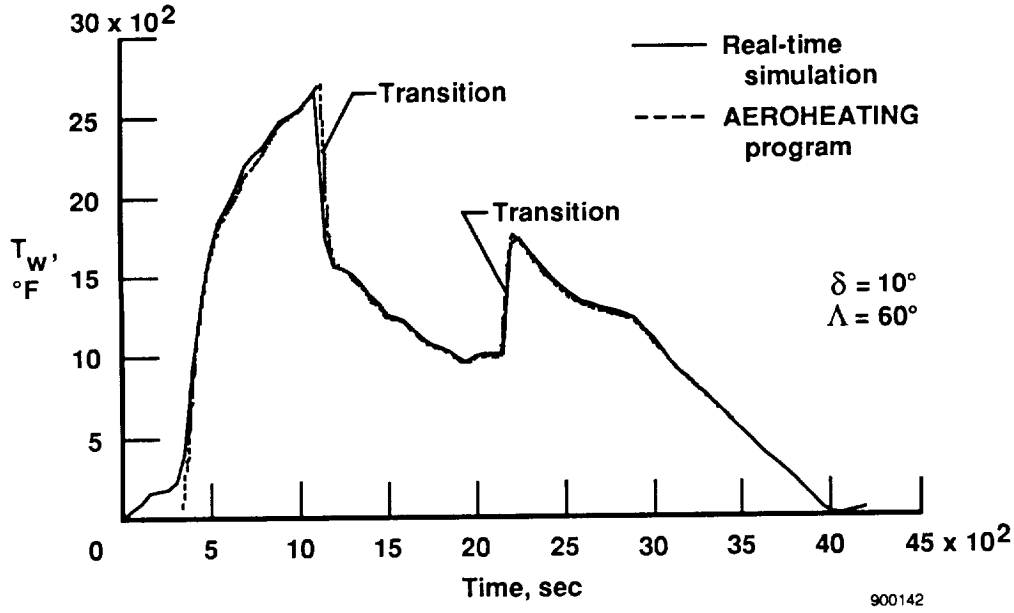

(p) Upper surface temperatures, $x = 24$ ft.

Figure 4. Concluded.

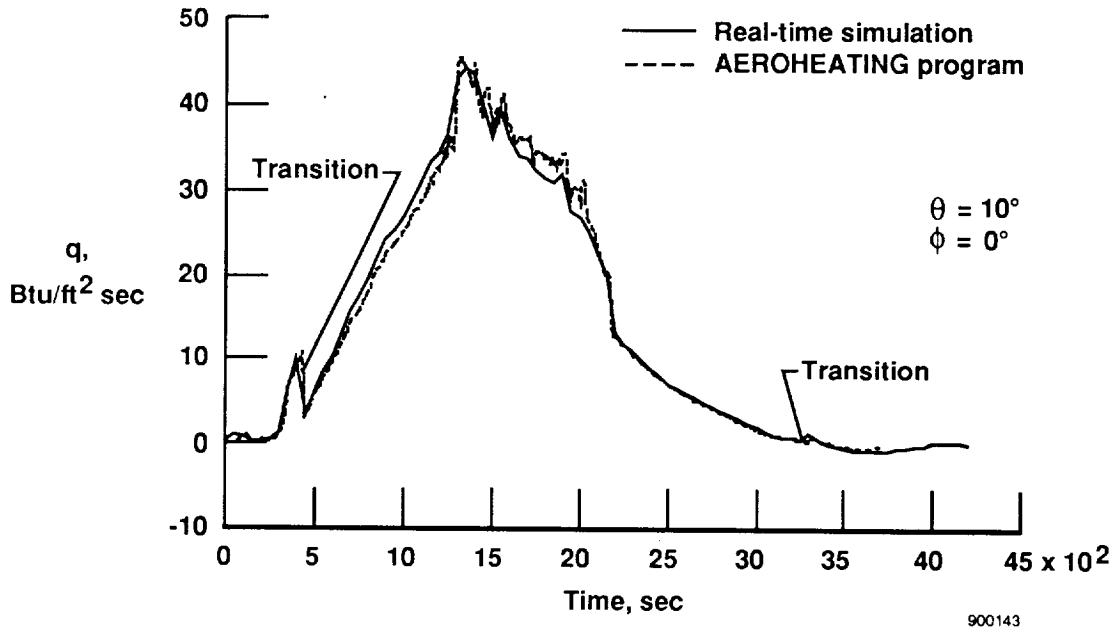

(a) Lower surface heating rates, x = 3 ft.

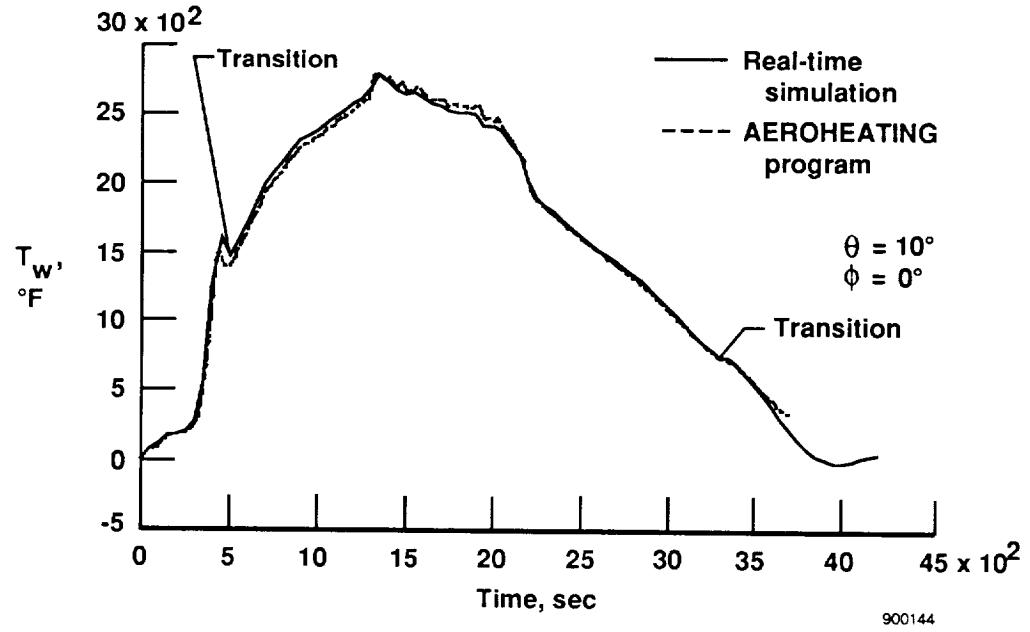

(b) Lower surface temperatures, x = 3 ft.

Figure 5. Heating rates and temperatures from the real-time simulation compared with values calculated by the AEROHEATING program for conical flow.

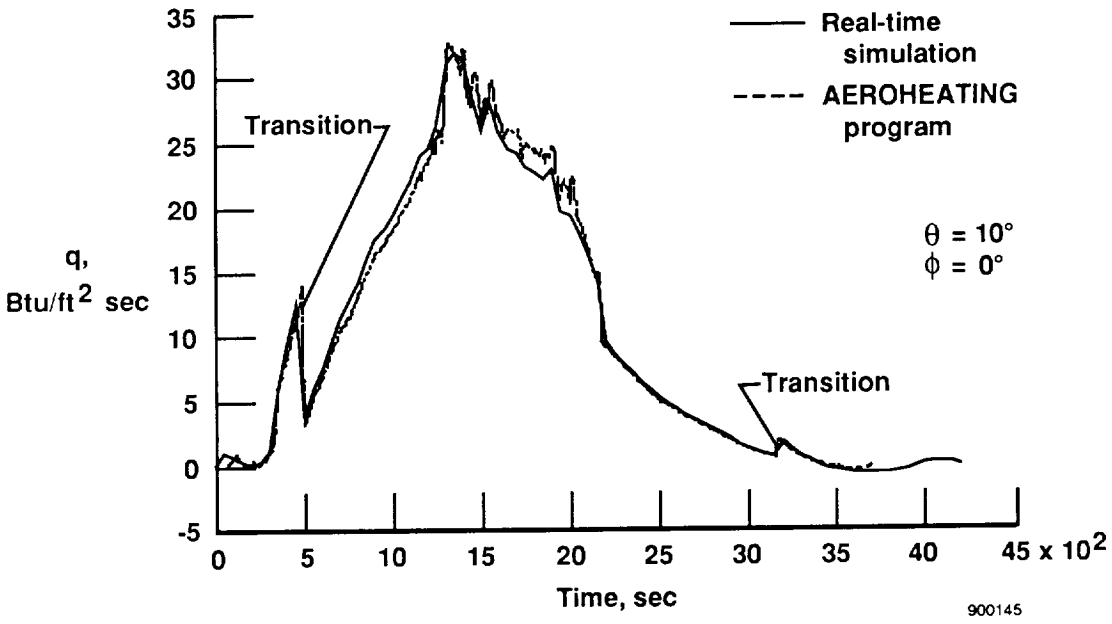

(c) Lower surface heating rates, $x = 6$ ft.

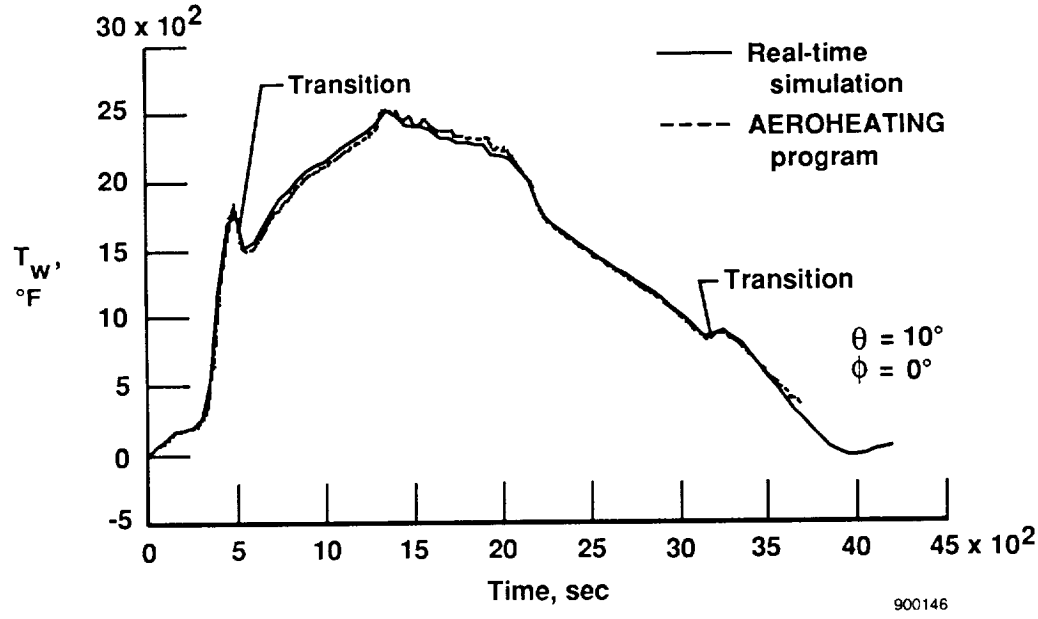

(d) Lower surface temperatures, $x = 6$ ft.

Figure 5. Continued.

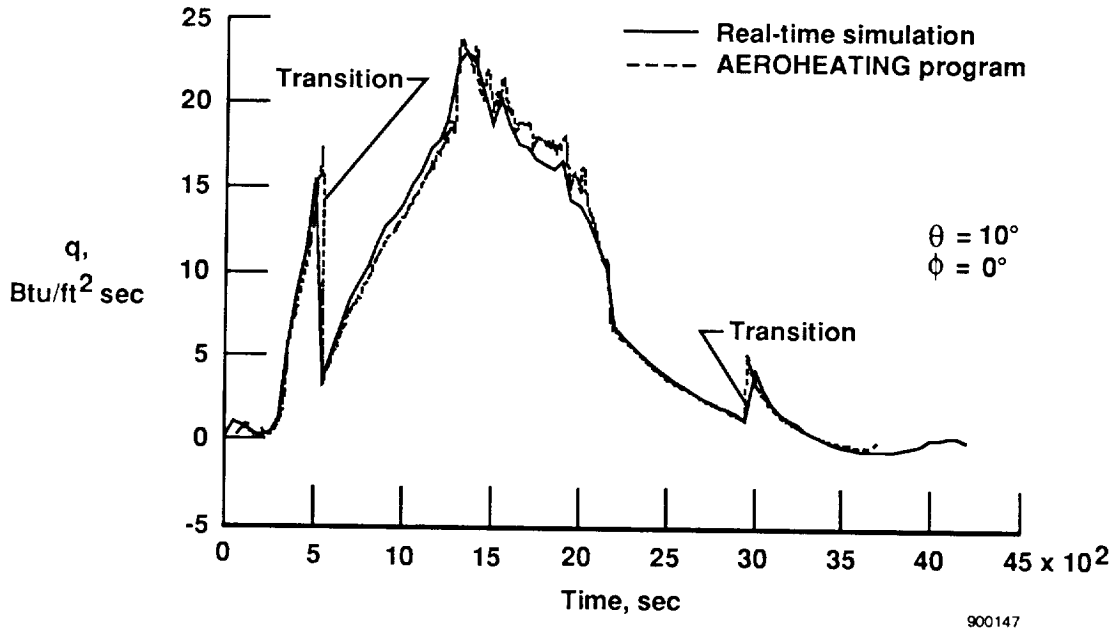

(e) Lower surface heating rates, x = 12 ft.

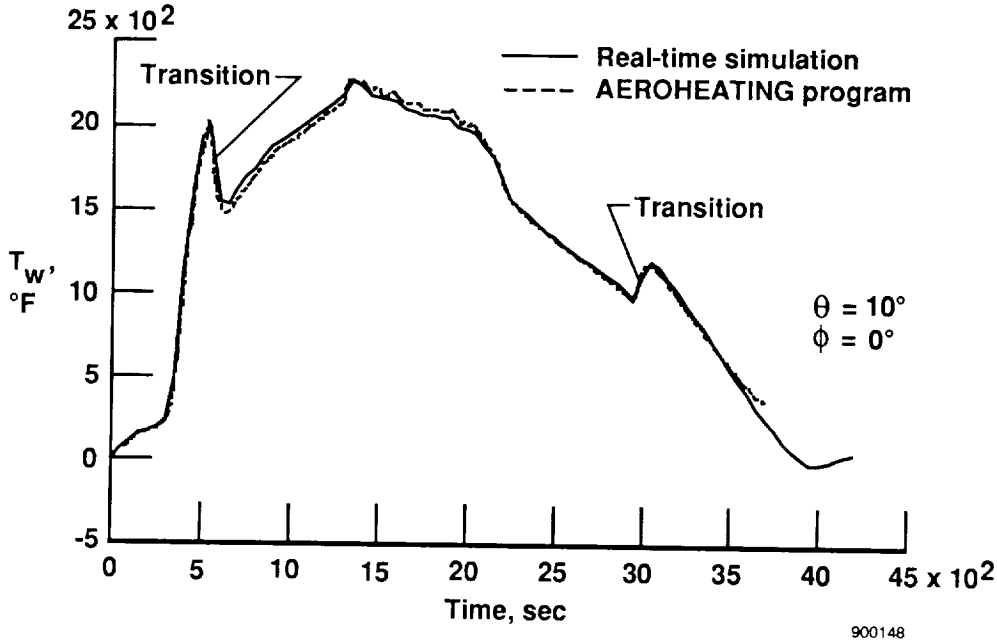

(f) Lower surface temperatures, x = 12 ft.

Figure 5. Continued.

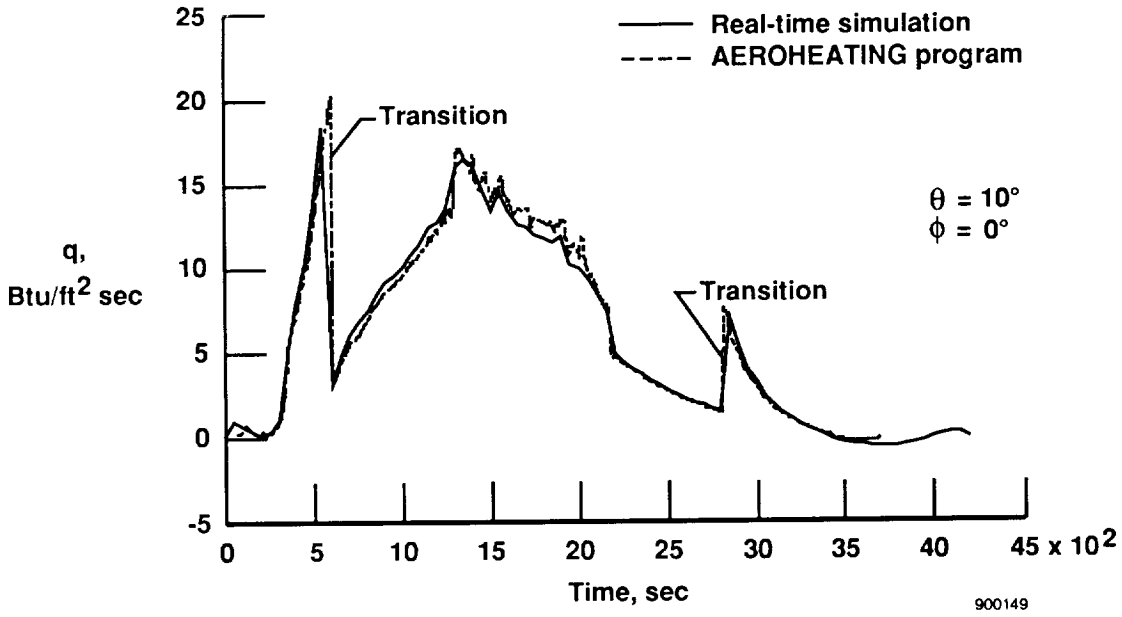

(g) Lower surface heating rates, x = 24 ft.

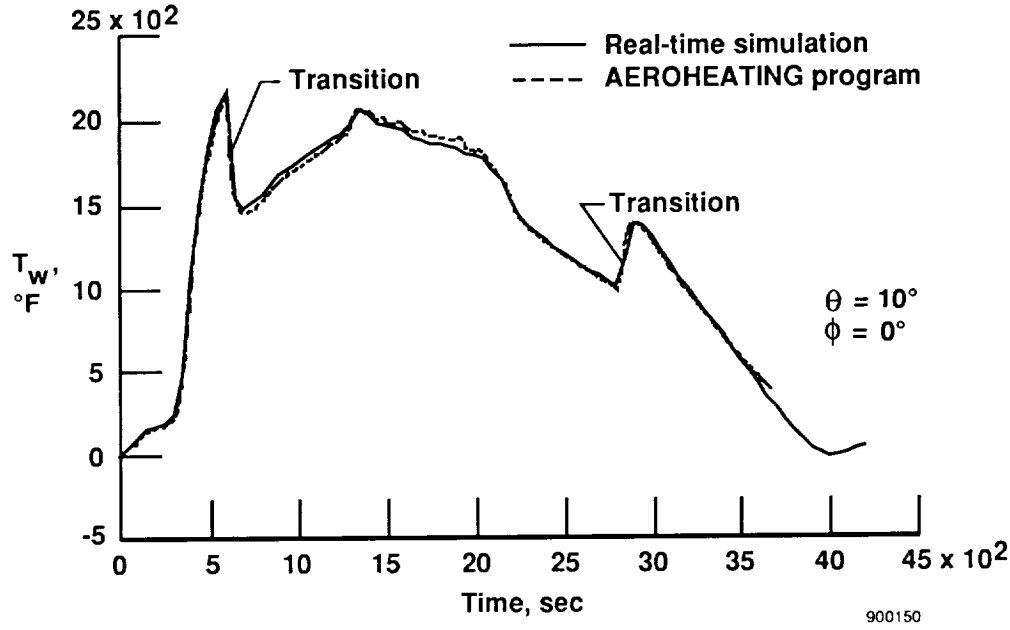

(h) Lower surface temperatures, x = 24 ft.

Figure 5. Continued.

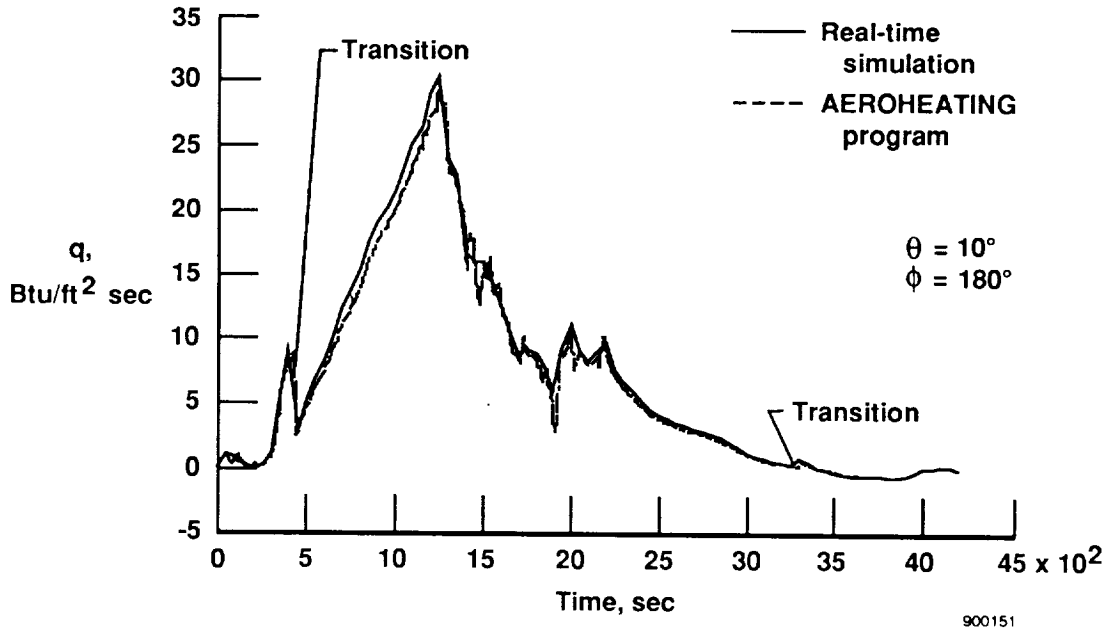

(i) Upper surface heating rates, $x = 3$ ft.

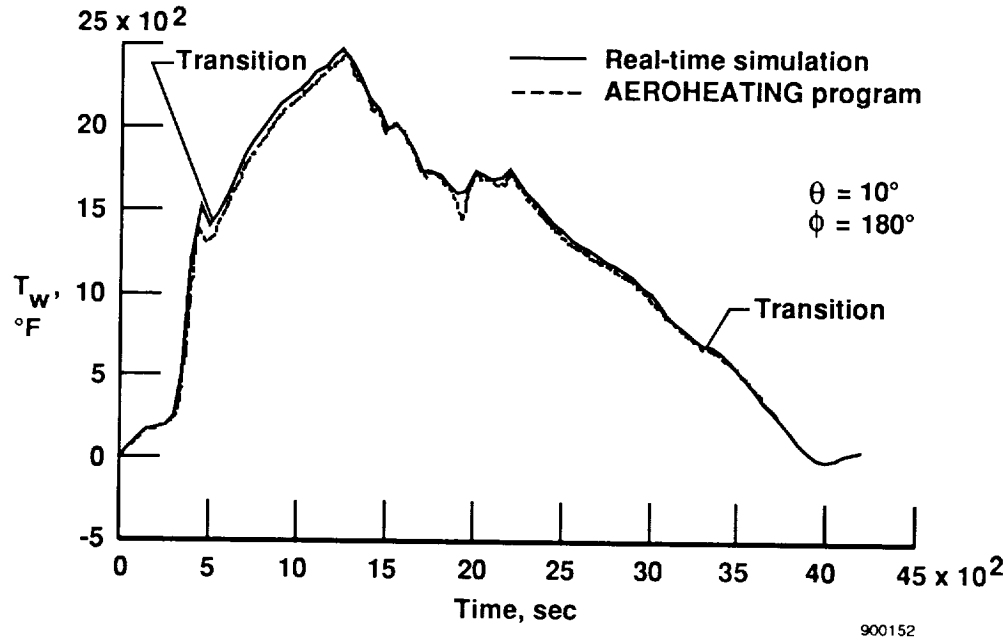

(j) Upper surface temperatures, $x = 3$ ft.

Figure 5. Continued.

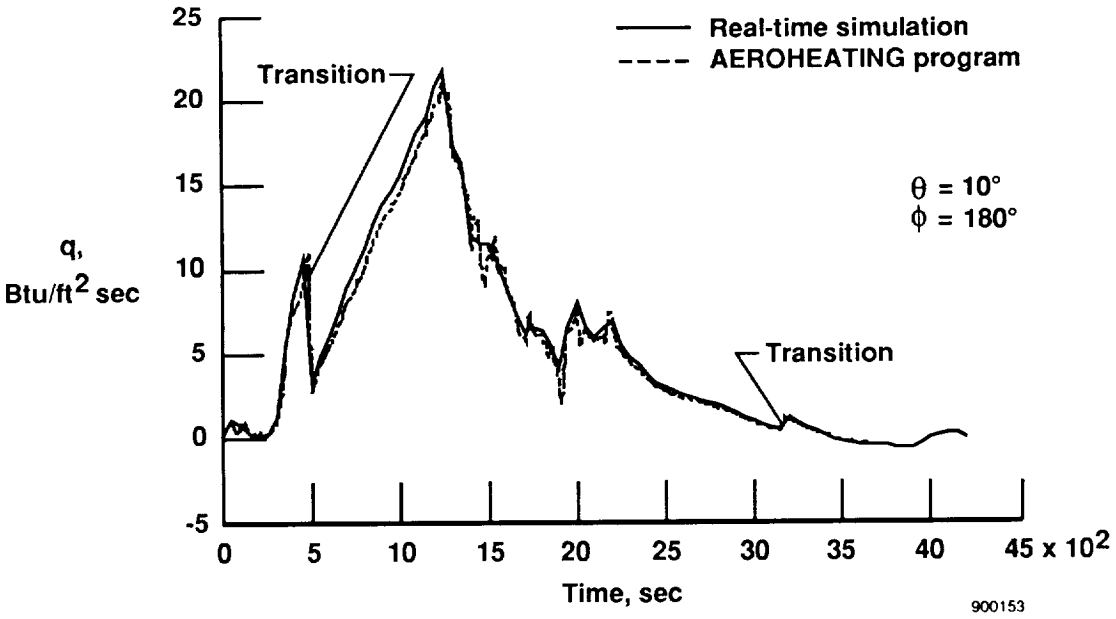

(k) Upper surface heating rates, x = 6 ft.

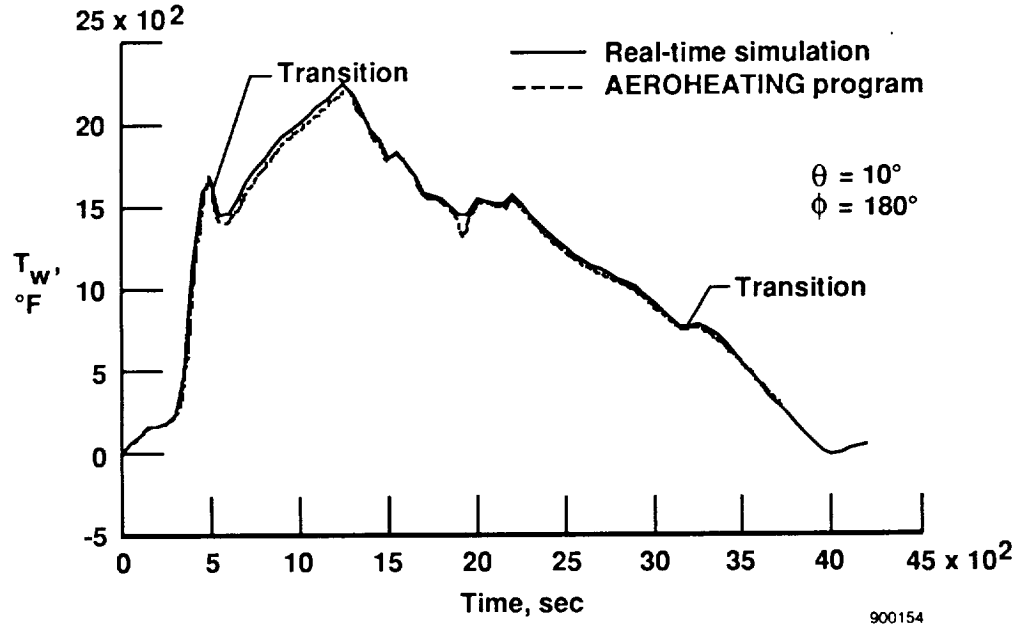

(l) Upper surface temperatures, x = 6 ft.

Figure 5. Continued.

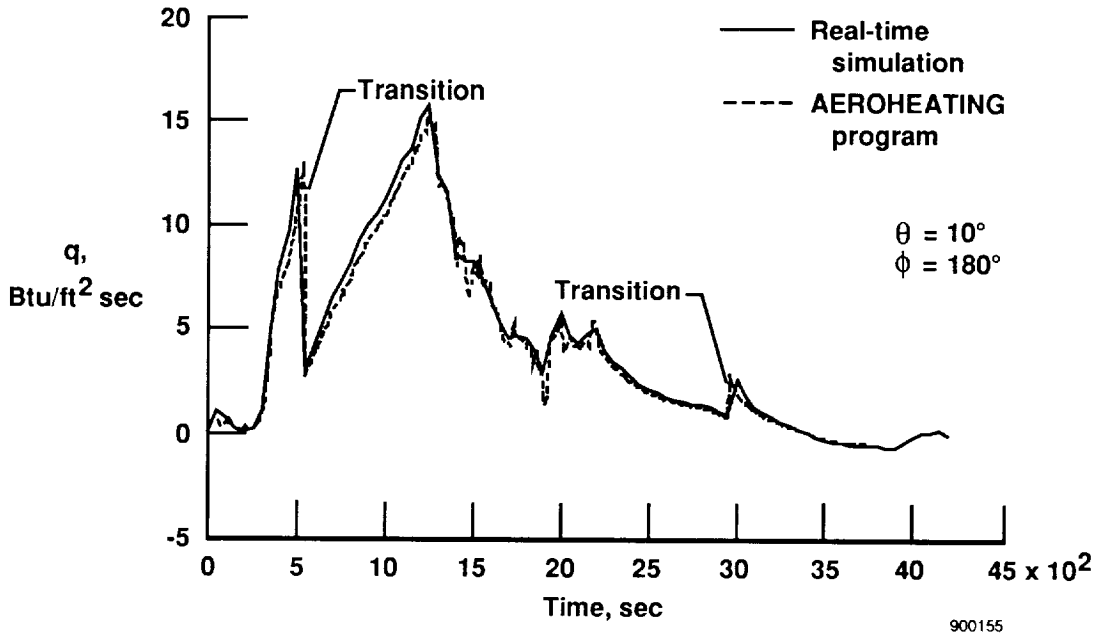

(m) Upper surface heating rates, x = 12 ft.

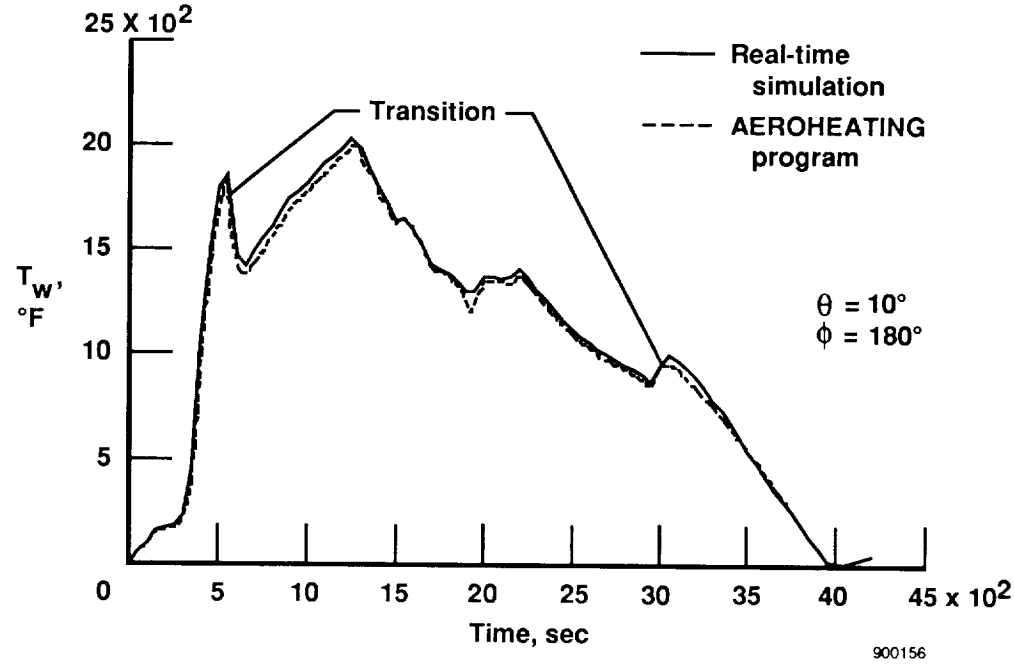

(n) Upper surface temperatures, x = 12 ft.

Figure 5. Continued.

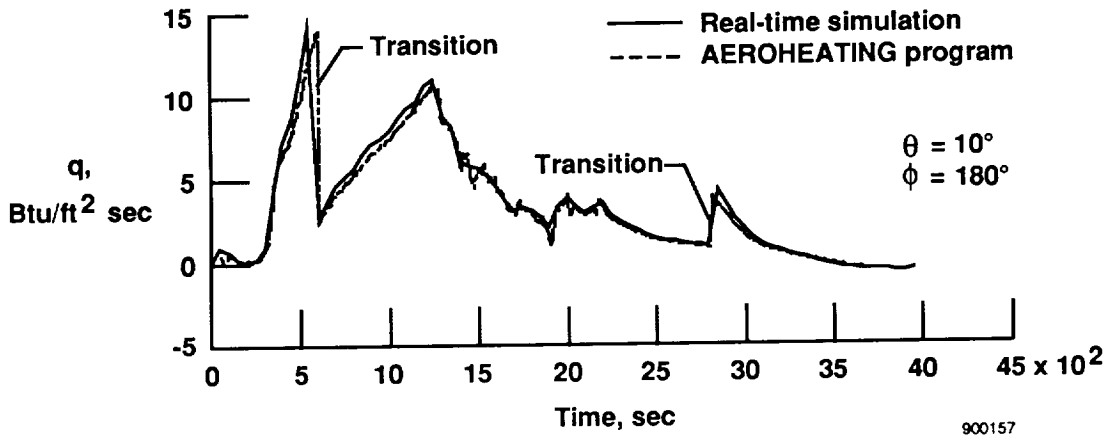

(o) Upper surface heating rates, x = 24 ft.

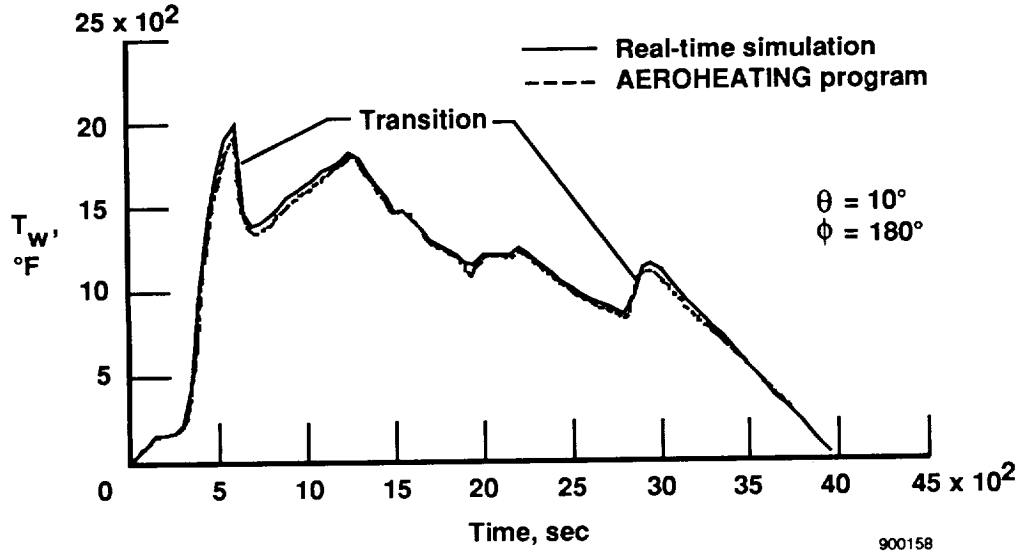

(p) Upper surface temperatures, x = 24 ft.

Figure 5. Concluded.

NASA
National Aeronautics and Space Administration

Report Documentation Page

1. Report No.	2. Government Accession No.	3. Recipient's Catalog No.
NASA TM-4222		

4. Title and Subtitle

Real-Time Aerodynamic Heating and Surface Temperature Calculations for Hypersonic Flight Simulation

5. Report Date: September 1990

6. Performing Organization Code:

7. Author(s)

Robert D. Quinn and Leslie Gong

8. Performing Organization Report No.: H-1602

10. Work Unit No.: RTOP 505-63-31

9. Performing Organization Name and Address

NASA Ames Research Center
Dryden Flight Research Facility
P.O. Box 273, Edwards, CA 93523-0273

11. Contract or Grant No.:

13. Type of Report and Period Covered: Technical Memorandum

12. Sponsoring Agency Name and Address

National Aeronautics and Space Administration
Washington, DC 20546-0001

14. Sponsoring Agency Code:

15. Supplementary Notes:

16. Abstract

A real-time heating algorithm has been derived and installed on the Ames Research Center Dryden Flight Research Facility real-time flight simulator. This program can calculate two- and three-dimensional stagnation point surface heating rates and surface temperatures. The two-dimensional calculations can be made with or without leading-edge sweep. In addition, upper and lower surface heating rates and surface temperatures for flat plates, wedges, and cones can be calculated. Laminar or turbulent heating can be calculated, with boundary-layer transition made a function of free-stream Reynolds number and free-stream Mach number. Real-time heating rates and surface temperatures calculated for a generic hypersonic vehicle are presented and compared with more exact values computed by a batch aeroheating program. As these comparisons show, the heating algorithm used on the flight simulator calculates surface heating rates and temperatures well within the accuracy required to evaluate flight profiles for acceptable heating trajectories.

17. Key Words (Suggested by Author(s))	18. Distribution Statement
Aerodynamic heating Real-time simulation	Unclassified-Unlimited Subject category - 34

19. Security Classif. (of this report)	20. Security Classif. (of this page)	21. No. of Pages	22. Price
Unclassified	Unclassified	44	A03

NASA FORM 1626 OCT 86

For sale by the National Technical Information Service, Springfield, Virginia 22161

NASA-Langley, 1990